Review

Understanding Urban Cooling of Blue-Green Infrastructure: A Review of Geospatial Data and Planning Optimization Methods for Mitigating Urban Heat Islands

Grzegorz Budzik *, Marta Sylla, Tomasz Kowalczyk

Posted Date: 20 November 2024

doi: 10.20944/preprints202411.1459.v1

Keywords: blue-green infrastructure; urban cool island; urban heat island; remote sensing; simulation; computational fluid dynamics; field measurements; digital twin

 doi:10.20944/preprints202411.1459.v1

Review

Understanding Urban Cooling of Blue-Green Infrastructure: A Review of Geospatial Data and Planning Optimization Methods for Mitigating Urban Heat Islands

Grzegorz Budzik [1,] *, Marta Sylla [2] and Tomasz Kowalczyk [3]

[1] PhD student in the 6th edition of the implementation doctorate programme---Ministry of Science and Higher Education; Wroclaw University of Environmental and Life Sciences, Department of Environmental Protection and Development, Grunwaldzki Sq. 24, 50-363 Wrocław, Poland
[2] Wroclaw University of Environmental and Life Sciences, Institute of Spatial Management, Grunwaldzka Str. 55, 50-357 Wrocław, Poland
[3] Wroclaw University of Environmental and Life Sciences, Department of Environmental Protection and Development, Grunwaldzki Sq. 24, 50-363 Wrocław, Poland
* Correspondence: grzegorz.budzik@upwr.edu.pl

Abstract: Many studies aim to assess the characteristics of blue-green infrastructure (BGI) that influence its cooling potential. Commonly used methods include satellite remote sensing, numerical simulations, and field measurements, each defining different cooling efficiency indicators. However, the methodological diversity creates uncertainties in optimizing BGI planning and management. This gap was addressed through a literature review, examining how BGI cools urban space, which spatial data and methods are most effective, which methodological differences may affect the results, and what are current research gaps and innovative future directions. Results suggest that differences in conclusions may arise from geographic and seasonal variations, as well as the spatial resolution of data, model scale, BGI delineation method, cooling range calculation approach, and urban morphology differences. The most influencing BGI characteristics include object size, vegetation fraction, density, height and multi-layering, foliage density, and spatial connectivity. The role of shape complexity remains uncertain across methodological approaches. Future research should prioritize the effects of urban morphology on BGI characteristics effectiveness and explore innovative approaches like Digital Twin technology for BGI management optimization. This paper comprehensively integrates key information related to BGI's cooling capabilities, serving as a useful resource for both practitioners and researchers to support resilient cities development.

Keywords: blue-green infrastructure; urban cool island; urban heat island; remote sensing; simulation; computational fluid dynamics; field measurements; digital twin

1. Introduction and Background

Climate change is causing increasingly frequent, intense, and prolonged heat waves (HWs) [1, 2, 3], which severely impact human society, quality of life, mortality [4, 5, 6, 7], the economy [8], and ecosystems [9, 10]. In cities, which feature unique land-use morphology and specific relationships between incoming and outgoing energy flows in the surface system, this trend is intensified by the formation of urban heat islands (UHI) [11, 12, 13, 14]. Urban conditions, along with population aging, high population density, and concentrated infrastructure, make cities especially vulnerable to HWs' negative effects.

Spatial planning can regulate urbanization processes to mitigate HWs-related risks [15, 16, 17, 18, 19, 20, 21]. Within this sector, and in conjunction with landscape architecture, economics, and

 doi:10.20944/preprints202411.1459.v1

ecological engineering, the concept of ecosystem services has emerged. This concept represents the multidimensional benefits people gain from urban natural capital, based on the blue-green infrastructure (BGI) [22, 23, 24, 25, 26, 27, 28, 29, 30]. In this context, BGI was developed as a tool to counteract the negative effects of climate change, including UHI. The BGI consists of: (1) natural and artificial hydrographic elements, such as rivers, reservoirs, wetlands, and marshes; (2) all vegetated areas, including public parks and gardens, forests, squares, etc.; (3) vegetation-based hydrological-engineering solutions, including rain gardens, green roofs, and retention-infiltration basins [31, 32].

The literature includes numerous studies evaluating the effectiveness of BGI in mitigating UHI, using related terms such as Park Cool Island, Water Cool Island, and Urban Cool Island (UCI), that refer to phenomena where specific BGI components have lower temperatures than impervious surfaces [33, 34, 35, 36, 37, 38]. These studies have assessed BGI characteristics for their cooling potential, supporting sustainable spatial policies [39, 40, 41]. Unfortunately, the variety of research methods may limit optimal implementation, creating uncertainty and confining conclusions to local findings only [42]. The main categories of methods for assessing BGI effectiveness include: (1) on-site air temperature (T-air) measurements to evaluate "air" UHI mitigation; (2) remote sensing of land surface temperature (LST) related to surface UHI (SUHI), often using satellite data; and (3) numerical modeling of T-air at micro-, local, and mesoscale levels [13, 42, 43, 44]. Moreover, it is notable that primary thermal data sources on urban areas, like LST and T-air, are not correlated [45, 46, 47, 48, 49, 50, 51]. Additionally, numerous indicators have emerged over time, defining BGI's cooling potential in various ways.

This methodological diversity increases uncertainty in forming conclusions about effective BGI design, as it can become a key factor—alongside geographical, climatic, and weather conditions—in creating variation in results. Consequently, for example, research based on T-air generally indicates that vegetation provides a better cooling effect than water [52, 53, 54, 55, 56], while LST-based studies show the opposite [57, 58, 55]. Moreover, some studies indicate that the complexity of BGI shape may positively influence cooling potential [59, 60, 61, 62, 63], while others suggest a negative impact [39, 41, 58, 64, 65]. Furthermore, notable variation exists within each method type, where: (1) satellite remote sensing results show BGI cooling ranges between 18 and 4,000 m, depending on data sources and LST downscaling level [59, 66, 67, 68]; (2) numerical simulations report cooling effectiveness from <1 to 18.4 °C, even after standardization based on vegetation fraction [42]; and (3) T-air field measurements indicate maximum cooling ranges of 180–860 m, with intensity levels between 0.14–8.8 °C [34, 69, 70, 71, 72, 73, 74].

For optimal planning and management of BGI, it is essential to organize and systematize existing research findings, including the potential impact of different research methods and data types. The wide variety of research techniques also points to the need for unified methodological frameworks to optimize BGI planning and management. Given advances in computational capabilities, these frameworks should leverage promising technologies such as Artificial Intelligence (AI), Big Data (BD), and the Internet of Things (IoT), which have the potential to enhance decision-support tools for BGI towards a more holistic approach. This framing can aid decision-makers and practitioners in interpreting results, and help researchers identify existing gaps and the most promising future research directions, ultimately leading to more effective BGI development strategies and stronger urban resilience against HWs.

In light of the aforementioned issues and uncertainties, the primary aim of this article is to systematize knowledge on the use of geoinformatics tools and spatial data in studying the cooling potential of BGI for spatial planning, through:

1. Presenting the mechanisms behind the formation of BGI's cooling abilities;
2. Discussing the most effective BGI features that positively impact cooling potential regardless of method;
3. Examining the characteristics of spatial data and geoinformatics methods used in analyzing BGI's cooling effects, with attention to potential impacts on result variability;
4. Proposing promising future research directions for optimizing BGI planning and management processes.

 doi:10.20944/preprints202411.1459.v1

2. Materials and Methods

The methodology is based on a literature review, focusing on four areas: remote sensing, numerical simulations, field measurements, and emerging technologies. Literature searches were conducted on Google Scholar, Web of Science, and Scopus, up to November 2024, using keywords related to the quantitative assessment of urban BGI cooling by common methods. Various combinations of the following phrases were used for searching titles, keywords, and abstracts: "green", "blue", "infrastructure", "water", "vegetation", "city", "urban", "heat island", "cooling", "cooling island", "cooling potential", "cooling effect", "air temperature", "land surface temperature", "factors", "method", "technology", "modeling", "smart cities", "remote sensing", "simulation", "field measurements", "transect", "traverse", "morphology", "local climate zones", and "digital twin".

The review included 287 references, selected for their relevance to: mechanisms and key features affecting BGI cooling effectiveness, characteristics of methods for quantifying BGI effectiveness that may influence the magnitude of cooling, and future research directions related to BGI management. Once the literature was selected, information was gathered at a progressive level (titles, then abstracts, keywords, and finally full texts), following criteria that: (1) the study is urban-focused, and (2) for objectives 2 and 3, it quantitatively assesses BGI features.

This review addresses BGI planning and management comprehensively—from current urban thermal assessment methods and mechanisms shaping BGI cooling to BGI characteristics that enhance cooling potential, considering both BGI-specific features and urban morphology. It also details geoinformatics methods for evaluating BGI's cooling, covering BGI representation models, cooling potential metrics, spatial data sources, and potential tool development directions with a focus on promising technologies.

3. Existing Methods for Assessing the Thermal Characteristics of Urban Areas

To better understand how BGI cools urban spaces, it is essential to outline basic concepts describing urban thermal characteristics, particularly the UHI phenomenon. The UHI effect can arise from climatic processes within both the Urban Boundary Layer (UBL) and the Urban Canopy Layer (UCL) [75,76]. This effect is most intense under anticyclonic conditions, especially during heatwaves, when increased solar radiation raises the energy stored in the urban environment, and at night, when heat release from urban surfaces becomes the primary contributor [75, 77]. UHI studies focus on two main areas: (1) "air" UHI, describing thermal differences within the atmospheric boundary and canopy layers, and (2) "surface" UHI (SUHI), analyzing temperature contrasts between urbanized and non-urbanized surfaces [13,43,44].

Measurements of the atmospheric UHI involve the use of sensors on fixed meteorological stations or mobile traverses to assess T-air differences within the UCL, or more advanced platforms such as tall towers, radiosondes, or aircraft-mounted temperature sensors to study the UBL heat island [44,78–80]. Relying solely on ground station T-air measurements can be inadequate for capturing fine-scale temperature variations within cities due to their sparse spatial distribution, often leading to an underestimation of temperature effects [81]. However, with self-programmed measurements, it is possible to track the actual intensity of the UHI in dense time series and vertical profiles.

Conversely, SUHI research heavily relies on satellite-based thermal remote sensing data, affording consistent and replicable evaluations of LST dynamics [45,82,83]. LST reflects the energy exchange between the land surface, atmospheric insulation, and solar radiation [84–86]. This process influences near-surface T-air, evapotranspiration, and atmospheric humidity [87], affecting perceived temperature [88]. However, relying solely on LST may be not sufficient for capturing the complex thermal dynamics of urban environments. Thermal sensors indirectly gauge temperature of the outermost layer of urban surfaces (tree canopies, rooftops etc.) by detecting upward long-wave radiation, which shaded areas under e.g., buildings and trees being undetectable [89,90], and various thermodynamic and radiative properties significantly impacting the detection [43,45,49].

 doi:10.20944/preprints202411.1459.v1

Additionally, atmospheric absorption can consume radiation [48], and some atmospheric radiation may reach sensors without directly interacting with the surface [43].

In the cities, LST can be completely different from T-air which plays an important role in energy balance [45,91]. While some studies have confirmed a general relationship between LST and T-air in coarse scales [46,92–100], this cannot be applied to the morphologically complex urban spaces, due to solar intensity, surface moisture, near-surface atmospheric conditions, wind, clouds, shading, sky view factor, and sensor view angle [45–51]. These factors, along with sparse station T-air measurements, lack of sensor homogeneity, and coarse spatial resolution of model-derived urban T-air data, prevent the estimation of T-air from LST in urban environments [101–104].

Alongside real-world measurements, the literature also identifies an additional UHI research approach—numerical simulations of T-air and other urban atmospheric characteristics [42]. Commonly used approaches within this methodology include local Computational Fluid Dynamics (CFD) [105,106] models and Energy Balance Models (EBM) [42, 107, 108], as well as mesoscale atmospheric models, such as WRF [42,109–111]. The most well-known CFD models include: OpenFOAM, FLUENT, STAR-CCM+, PHOENICS, and ENVI-met. In the case of EBMs, notable models include RayMan, SOLWEIG, green-CTTC, and TEB-Veg [108].

Despite the variety of methods available for assessing UHI and UCI, the most effective and, therefore, the most commonly used are: field measurements, satellite remote sensing, and CFD numerical simulations (for UCI primarily using ENVI-met).

4. Factors Determining the Cooling Potential of BGI

4.1. Micro-Scale Properties of BGI Affecting Cooling Potential

Through mechanisms like transpiration, shading, absorbing solar radiation for photosynthesis and modification of airflow, vegetation plays a pivotal role in urban energy balance, alleviating the UHI effect [77,112–115]. Evapotranspiration through BGI development can replace sensible heating with latent heating, leading to evaporative cooling, effectively lowering both surface and ambient temperatures [112]. The cooling process of urban space by vegetation is shown in Figure 1.

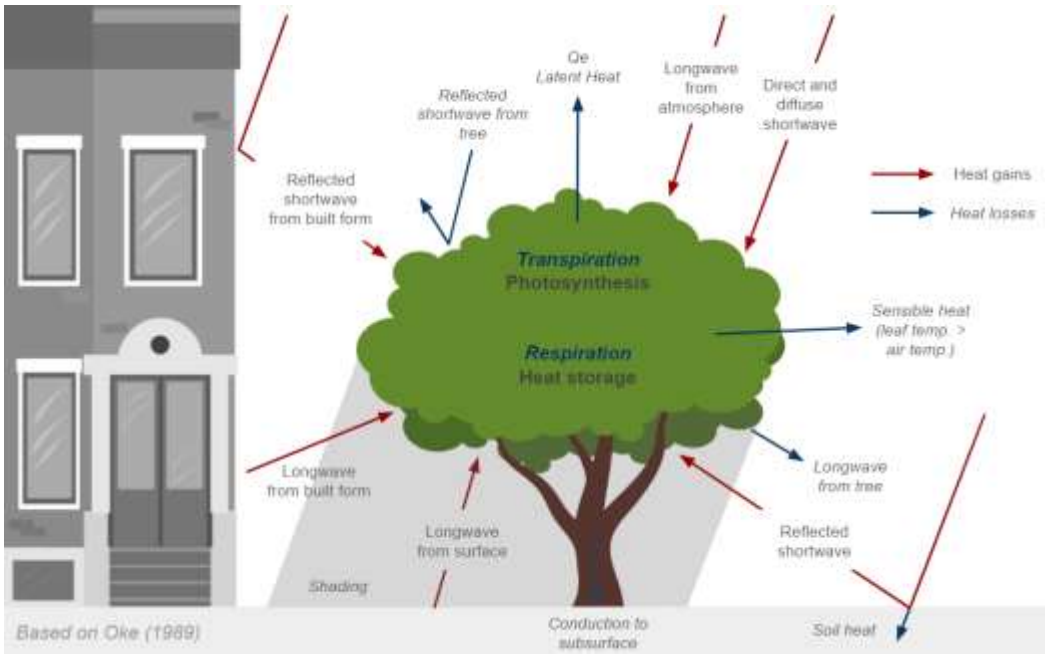

Figure 1. Schematic of urban space cooling by vegetation. Based on Oke [116].

The cooling potential of transpiration can vary based on factors such as plant species, leaf characteristics, stomatal resistance, and soil conditions [70, 117, 118]. Additionally, transpiration rates are influenced by weather and climate conditions, with plants actively regulating stomatal openings

 doi:10.20944/preprints202411.1459.v1

to manage heat stress and water loss [77, 119]. Prolonged heat waves and drought conditions can reduce the effectiveness of evaporative cooling [77,120] and may cause vegetation to release carbon dioxide to the atmosphere [121]. Urban vegetation also provides shading, that intercept solar radiation, limiting heat absorption and minimizing heat re-radiation by urban surfaces [115, 116]. Shading effectiveness depends on factors like leaf size and density, and canopy density [122,123]. Additionally, greenspaces modify local wind patterns, facilitating convective heat exchange and dissipating heat flux, further enhancing cooling effects [75]. In this context, studies suggest that the dispersed arrangement of tree canopies may be more effective [124,125], additionally preventing heat retention, and maintaining optimal relative humidity levels, especially at night [77]. Moreover, vegetation indirectly assists climate cooling by filtering pollutants through dry deposition and pollutant absorption [77]. These processes reduce atmospheric scattering and absorption of radiation, impacting the radiation balance and T-air [126].

Studies on the cooling benefits of BI are fewer compared to greenspace, focusing primarily on daytime temperature effects and LST differences, which may not fully capture the conversion of sensible heating to latent heating [77,127]. BI can reduce the daily UHI effect due to water's high heat capacity and low thermal conductivity, as well as evaporation properties, leading to the so-called "thermostatic effect" [75,128]. Shading, reflectance, and thermal inertia play significant roles in BI cooling [75,113], with wind velocity enhancing convective heat transfer and evaporation rates [129]. Dynamic water bodies like rivers carry heat downstream, affecting local temperatures [130], while static water bodies, like lakes, exhibit thermal stratification, influencing their cooling efficiency based on their size and depth [75,131].

Comparative assessments of greenspace and bluespace integrated cooling abilities are rare in climate studies. Some research indicates significant cooling effects within street canyons with access to riparian greenery, while also showing variability in cooling potential based on factors such as river water temperature, incident solar radiation, wind speed, and relative humidity [132]. Moreover, riparian vegetation has been shown to reduce the net radiation balance and T-air over streams [133]. However, vegetation can create windbreaks, promoting moisture accumulation above water surfaces, which may lead to the formation of warm, humid pockets in the 'quiet zone' downwind, negatively impacting cooling efficiency [134].

4.2. Local-Scale Properties of Bgi Affecting Cooling Potential

Studies on UCI extent most frequently identify BGI size [34, 135, 136, 137, 138], vegetation intensity and quality [139–142] (with grasslands showing the weakest efficiency [41]), adequate irrigation [33,41,143], proportion of forest vegetation [40], and the presence of surface water within BGI boundaries [41,144–146] as the features most strongly influencing the UCI extent provided by BGI in local scale. A key factor influencing the overall cooling effect may also be surface roughness, which depends on vegetation arrangements and affects ventilation characteristics [77]. Larger BGIs can create greater temperature and humidity contrasts with built-up areas, enhancing the park-breeze effect [72, 77, 147, 116]. Foliage and vegetation condition may enhance cooling effects by: (1) enhancing evaporative cooling [70, 112, 118] due to intensified photosynthesis [77, 120], (2) reducing solar radiation absorption due to shading [116,122,148], and (3) boosting convective cooling, by raising canopy surface roughness [75, 77]. Better efficiency in areas integrating greenspace with water may result from the synergistic capabilities of evaporative cooling and reduced solar radiation absorption by BI through shading by vegetation, which, along with internal convection processes and water mixing in reservoirs, further enhances BI's ability to absorb surrounding heat [77]. Additionally, the proximity of BI ensures better access to groundwater, strengthening the resilience of GI to drought and increasing the cooling capacity of vegetation [117,119,120].

The complexity of BGI shapes can either positively [59–63] or negatively [39, 41, 58, 64, 65] impact the cooling range, depending on the adopted scale [58], climatic zone, or type of development. This complexity can weaken the cooling effects of vegetation located at the boundary of complexly shaped BGI areas by amplifying thermal stress, leading to stomatal closure [77,148], which can be dependent on surrounding development settings. Additionally, the efficiency of surface

 doi:10.20944/preprints202411.1459.v1

water compared to vegetation remains a topic of debate [149,150]—it may be greater in terms of LST [55, 57, 58, 63, 151] and lower in terms of T-air [52–56]. Regarding BI, the size and shape also influence its cooling efficiency, with larger bodies with complex shapes generally providing more significant cooling [57,58,152]. Latitude, seasonal, and diurnal variations also affect cooling intensity, which is stronger in lower latitudes and varies throughout the day and year [153–155].

The spatial configuration and composition may also influence the UCI intensity [156,157]. BGI objects situated in the highest spatial density may interact with their neighboring facilities, limiting each other's cooling zones [138, 158, 159], which demonstrates the collective cooling capabilities of small spatially concentrated BGIs. In this context, the characteristics of BGI objects can be examined in terms of landscape metrics. The most significant feature may be the level of aggregation and connectivity of BGI objects [68, 160]. Additionally, the combination of edge density and patch density may exert a high influence on UCI [157]. Spatial arrangement has also proven to be important in case of BI, with large water bodies presenting a higher cooling effect compared to equally distributed small water bodies [161].

The examples of the discussed features are presented in Tables 1, 3, and 4.

4.3. Urban Morphology Impact

The cooling potential of BGI is influenced not only by its internal characteristics but also by the surrounding urban areas morphology [62, 129, 138, 162]. Through the modification of airflow, atmospheric heat transport, radiation balances, albedo, moisture availability, and surface heating potential [163], the built environment affects evaporative cooling [70, 112, 118] and convective cooling [75,77], regulating the intensity of the so-called park-breeze effect [72, 77, 116], which allows the transfer of cooler air to built-up areas due to the temperature difference between the BGI and the urban surfaces (Figure 2).

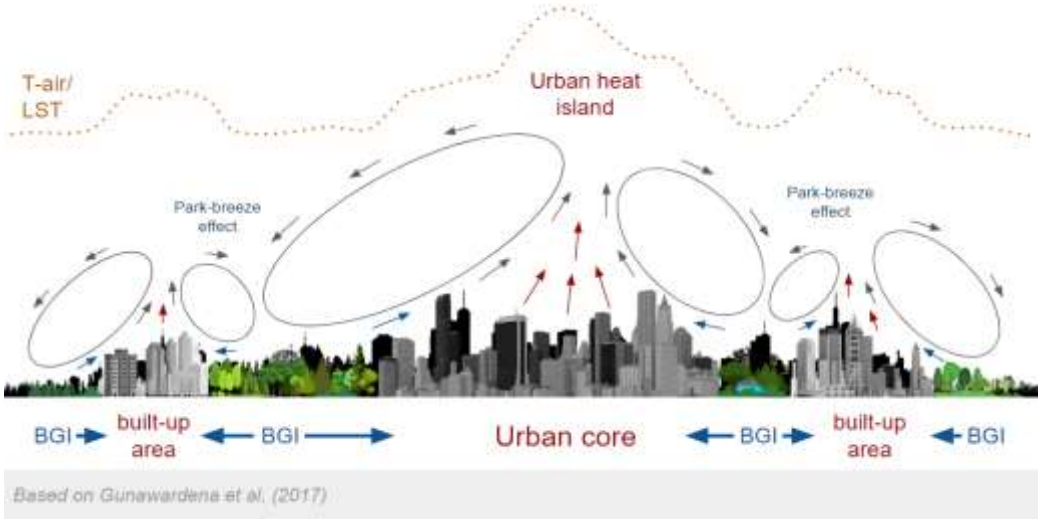

Figure 2. Diagram of the park-breeze effect mechanism. Based on Gunawardena et al. [77].

The primary factors by which building types influence BGI cooling potential are air humidity and temperature contrasts, which regulate the intensity of the park-breeze effect [72,77,116]. Urban structures also modify wind conditions, affecting the strength of convective cooling [164,165]. Additionally, urban development can induce thermal stress on plants, potentially leading to stomatal closure and limiting evaporative cooling during extreme temperatures [70, 114, 165], and can also impact drought risk, which reduces BGI cooling efficiency [70,166,167]. Thus, denser building patterns may both enhance the park-breeze effect [117, 165, 168, 169], as well as increase plant thermal stress and limit water access, ultimately diminishing cooling potential.

The most comprehensive model for classifying urban morphology in terms of characteristics relevant to BGI cooling capabilities (e.g., emissivity, reflectivity, conductivity, absorptivity, and

 doi:10.20944/preprints202411.1459.v1

sensible heat storage) is the Local Climate Zones (LCZ) classification system developed by Stewart and Oke [163]. This model enables the delineation of homogeneous urban areas based on surface structure and cover, building types, materials, and human activity. LCZs have a distinct screen-height temperature regime, particularly noticeable over dry surfaces during calm nights in areas with uniform landform [163]. In addition to screen-height temperature, LCZs also define homogeneous zones by air humidity regime [170] and local-scale urban ventilation performance [171], thus distinguishing urban spaces by their actual potential for BGI evaporative and convective cooling. Notably, initially designed to define UBL UHI more accurately [163,172,173], due to the consistent delimitation of homogeneous areas in terms of natural and artificial materials (like emissivity, reflectivity, conductivity, absorptivity and sensible heat storage capacity), LCZ can also be successfully applied in LST-based studies [43, 174, 175, 176, 177, 178, 179].

5. Characteristics of Selected Geoinformatics Methods and Spatial Data Used to Assess the Cooling Potential of BGI

5.1. UCI Studies Based on Satellite Remote Sensing

The remote sensing approach is based on LST. These data are typically obtained through satellite remote sensing using passive sensors that detect both the reflected shortwave radiation reflected from the land surface and the emitted longwave (thermal infrared) radiation [180].

5.1.1. Methods for Creating BGI Representation

In remote sensing studies, two primary types of BGI representation are distinguished: continuous and discrete. Continuous BGI representation is achieved through vegetation indices such as the normalized difference vegetation index (NDVI), which illustrate the spatial distribution and intensity of BGI presence. Here, each raster pixel is treated as an individual sample, making the analysis of BGI efficiency largely based on correlating the BGI raster with the LST raster [181]. Discrete representation, on the other hand, involves clearly defined boundaries for BGI areas, allowing differentiation between vegetation and surface water [59]. However, accurately delineating BGI boundaries can be challenging. Common methods include supervised classification and reclassification of vegetation indices (e.g., NDVI). In this model, each BGI feature is treated as a single sample. The method allows the use of predefined urban data (e.g., only publicly accessible green spaces). In SUHI analyses, less common representation methods have also emerged, offering unique advantages, such as the "cooling network and cooling source areas" model, which organizes information on BGI features through morphological spatial pattern analysis (MSPA) [156].

5.1.2. Methods for Assessing the Cooling Potential of BGI

The cooling extent directly influenced by BGI is challenging to evaluate, as it depends on both BGI characteristics and the thermal conditions of adjacent built-up areas [158, 182]. Common approaches focus on identifying the first turning point in the LST-distance function from the edge of a BGI feature [59, 64, 151, 166, 183, 184]. This approach mainly aims to define the cooling range of BGI (HCD), which ends at the first inflection point on the function, and cooling intensity (HCI), measured as the LST difference between the first turning point and the BGI boundary. Calculating these indicators typically involves various spatial analyses, with popular methods including the assessment of LST increase based on zonal means in buffer zones around BGI features [66, 166]. LST values can also be collected along straight lines extending outward from BGI boundaries, in cross-sections [59], to evaluate potential variations in UCI extent direction. More advanced techniques like the semivariance function [158, 185] or the use of watershed algorithms that treat LST as terrain elevation, where watersheds represent cooling zones, are also applied [138]. Surface-based methods are most effective, as they capture directional cooling influences, though validation against control measurements is essential for accuracy.

5.1.3. Remote Sensing data Used in UCI Studies

 doi:10.20944/preprints202411.1459.v1

The most commonly used data sources for LST calculations include the Landsat satellite series, the MODIS instrument, and ASTER [43]. The capability for thermal radiation detection began in 1982 with the launch of the Thematic Mapper (TM) sensor on the Landsat 4 satellite, which imaged the Earth's surface in thermal infrared at a spatial resolution of 120 m [186]. The latest generations of Landsat (8 and 9) can generate LST data using the Thermal Infra-Red Sensor (TIRS), which a resolution of 100 m, with the possibility of resampling to 30 m to match the bands of the Operational Land Imager (OLI) [187]. Since 2008, Landsat data has been freely available. A single image covers an area of 185 x 185 km, allowing for the analysis of entire urban areas based on data from a single time point. For Landsat 5, 7, 8, and 9, the revisit cycle for the same area is 16 days, with Landsat 8 and 9 having revisit schedules that enable increasing the temporal resolution to 8 days. This allows for the analysis of UCI changes over time with high frequency, enabling the recording of the impact of land use changes on urban thermal conditions. Landsat is one of the most effective sources of information on the thermal characteristics of urban areas.

The second most popular source of LST data is MODIS, an instrument mounted on the Terra and Aqua satellites [43,188–190], which were launched in 1999 and 2002. The temporal resolution of MODIS data is 1-2 days, which allows for the creation of high-frequency time series, but the spatial resolution is only 1 km, limiting the ability to conduct detailed analyses of the cooling potential of individual BGI objects. However, due to the large size of each image (a 2330 km wide strip), MODIS is widely used in studies of large areas [43,191,192]. Additionally, MODIS provides many ready-to-use products, including daytime and nighttime LST and emissivity data [193,194]. MODIS data is freely available.

Another source of LST data is ASTER, located on the Terra satellite [43,195]. These data were collected during the radiometer's operational period from 1999 to 2016. ASTER imaged the Earth's surface in 14 bands, with 4 of them capturing the thermal infrared spectrum at a spatial resolution of 90 m [196]. This instrument provides access to the Surface Kinetic Temperature product, available for both daytime and nighttime [43,197]. Like Landsat and MODIS, ASTER data are also freely available. However, these data are rarely used in studies of UCI extent.

In recent years, LST data from the ECOsystem Spaceborne Thermal Radiometer Experiment on Space Station (ECOSTRESS) sensor have gained increasing popularity [51, 198, 199]. This sensor was launched to the International Space Station (ISS) on June 29, 2018, with a temporal repeat cycle of 3-5 days, depending on latitude [200]. ECOSTRESS images the Earth's surface in five bands, providing LST with a spatial resolution of 38 m x 68 m, with a single image covering an area of 402 km (53°) [51]. The main advantage of ECOSTRESS data is the inclined, precessing ISS orbit, which allows for imaging the same area at different times of the day and night, enabling the analysis of diurnal variations [200]. Additionally, the five channels enable more accurate multispectral Temperature Emissivity Separation (TES) approaches for LST calculations [51,201]. ECOSTRESS data are freely available. Due to its relatively recent launch, these data have not yet been used to study the thermal effectiveness of BGI characteristics.

Additional useful data for BGI research include: PlanetScope SuperDove (free for research purposes, 3 m resolution, 8 bands, ideal for time-series BGI and vegetation health classification); WorldView (paid, up to 0.3 m resolution, 16 bands, excellent for BGI and artificial materials classification); IKONOS, QuickBird, GeoEye-1, Pleiades-1, SPOT-5/6/7, Gaofen, and SkySat (effective for BGI classification); Prisma (30 m hyperspectral data for vegetation species classification); EnMap (high-resolution hyperspectral data); Sentinel-5P (free, suitable for air pollution time-series mapping); Sentinel-2 (free, good for large-scale BGI classification and vegetation health assessments); and ERA5 (free, high temporal resolution weather model).

Examples of research results on BGI features affecting its cooling potential using remote sensing techniques are presented in Table 1.

Table 1. Examples of studies on BGI features affecting its cooling efficiency using satellite remote sensing (+ and - indicate the direction of the feature's influence on cooling potential; the multiplicity of the sign indicates the relative significance of the influence).

 doi:10.20944/preprints202411.1459.v1

Source	Satellite sensor	LST spatial resolution	LST retrieval method	Date and temporal resolution	Study region	BGI type	Cooling potential calculation method	Cooling potential values	Method for impact assessment	BGI characteristics studied	BGI most efficient characteristics
Sun et al. [66]	ASTER	15 m from 90 m	TES	daytime; 2007-08-08; 16 days	Beijing, China	Wetlands (15)	HCD: mean LST in 50 m buffer rings; HCI: temperature difference between HCDmin and HCDmax	HCDmax: 2500 m HCDmean: 963 m HCImax: 5.83 °C HCImean: 2.6 °C	Spearman rank correlation coefficient	Area, LSI, perimeter-area ratio (PARA), path-fractal dimension (PFD), distance to the city center (DCC)	**Area** HCD (+); HCI (-) **LSI** HCD (-); HCI (-) **DCC** HCD (+); HCI (-)
Shah, et al. [202]	Landsat 8 TIRS	30 m from 100 m	The mono-window algorithm (MW)	daytime; 2017-04-24,2017-01-02	Bengaluru, India	Green spaces (manually traced based on Google Earth) (262)	HCD: mean LST in 30 m buffer rings; HCI: temperature difference between BGI object border and HCDmax	HCDmean: 347 m HCImean: 2.23 °C	Multiple linear regression model	Area, LSI, NDVI of BGI, NDVI of buffer	**LSI** HCD (+) **NDVI of BGI** HCD (+)
Zhang et al. [166]	Landsat 8 (LST) LocaSpace Viewer (BGI)	100 m	The radiative transfer equation method (RTE)	daytime; 2021-08-02; 16 days	Xi'an, China	Comprehensive, ecological, theme and belt parks (40)	HCD: mean LST in 25 m buffer rings; HCI: temperature difference between BGI mean LST and HCDmax; park cold island efficiency (PCE), intensity (PCI), gradient (PCG)	HCImax: 4.44 °C HCImean: 2.22 °C	Pearson correlation coefficient	Composition: area, perimeter, water area, green area, impermeable surface area; Configuration: park shape index, patch density, edge density	**Area** HCI (++) **Perimeter** HCI (+) **Water area** HCI (+) **Green area** HCI (++); PCI(+) **Park shape index** HCI (+); PCI (+) **Patch density** PCE (+) **Edge density PCE** (+)
Garcia-Haro et al. [203]	Landsat 8 TIRS	30 m from 100 m	The emissivity corrected algorithm (EC)	21-06-2017; 24-06-2018; 20-06-2019; 22-06-2020	Barcelona, Spain	Urban parks (86)	HCD: mean LST in 10 m buffer rings; HCI: temperature difference	HCDmean: 91.98 m HCDmax: 280 m HCImean: 1.84 °C HCImax: 3.74 °C	Bivariate correlation and multiple linear regression analysis	Size LSI, proportion of green land cover, greenery composition,	**Greenery composition** (+) **Greenery area** (+) **Area** (+/-)

 doi:10.20944/preprints202411.1459.v1

						between BGI mean LST and HCDmax			urban surrounding characteristics	**LSI** (-)
Qiu et al. [59]	Landsat 8 TIRS and Landsat 5 TM	30 m from 100/120 m	–	daytime; 1998-08-23, 2009-08-21, 2019-08-17; 16 days	Changsha, China	Green spaces (53) and blue spaces (28)	HCD: LST sampling on eight straight lines from BGI object; HCI: temperature difference between BGI object border and HCDmax	HCDGImax: 340 m HCDGImean: 163.33 m HCIGImax: 3.54 °C HCIGImean: 1.8 °C HCDBImax: 370 m HCDBImean: 175.58 m HCIBImax: 5.04 °C HCIBImean: 2 °C	Logarithmic regression analysis; nonlinear surface fitting	Area, LSI	**Area** (+) **LSI** (+)
Bao et al. [158]	Landsat 8 TIRS and Landsat 5 TM	30 m from 100/120 m	MW	daytime; 2000, 2004, 2007, 2011, 2014	Baotou, Mongolia	Green spaces (screen visual interpretation) (9)	HCD: semi-variance function	HCD: 1600 m	Linear and nonlinear regression	Class Area (CA), Number of Patches (NP), LSI, Aggregation Index (AI), Shannon's Evenness Index (SHEI), Mean Patch Fractal Dimension (FRAC_MN), PARA, NDVI	**Area** (++) **NDVI** (+)
Yu et al. [41]	Landsat 7 TM and Landsat 8 TIRS SPOT5 (for BGI classification)	30 m from 120/100 m	RTE	daytime; 2000-07-23, 2013-04-04	Fuzhou, China	BGI (106 BGI and 329 GI (280 tree-based and 49 grass-based))	HCD: mean LST in 30 m buffer rings; HCI: temperature difference between BGI object border and HCDmax; cooling efficiency (HCE); Threshold value of efficiency (TVoE)	HCDmean: 104 m HCImean: 1.78 °C TVoE: 4.55 ha	Linear regression and hierarchical cluster analysis for dividing BGI into size-based groups	Area, LSI, fractal dimension index (FRAC), waterbody presence	**Area** (+) **Waterbody presence** (+) **LSI** (-)

 doi:10.20944/preprints202411.1459.v1

Xue et al. [204]	Landsat 8 TIRS	30 m from 100 m	The split-window algorithm (SW)	daytime; 2016-07-04	Changchun City, China	Wetlands (21)	HCD: mean LST in 50 m buffer rings; cooling capability index (CCI); normalized CCI; cooling efficiency index (CEI), normalized CEI	HCDmax: 1000 m HCDmean: 371.1 m HCImean: 2.74 °C	Spearman's Rho Correlations	Area, LSI, hydrologic connectivity, type (rivers, lakes, wetlands, green spaces)	**Area** (++) **LSI** (+) **Connectivity** (+) **Type: lakes** (+)
Du H. et al. [62]	Landsat 8 TIRS	30 m from 100 m	RTE	daytime; 2013-08-29	Shanghai, China	Green spaces (manually traced based on Google Earth)	HCD: mean LST in 10 m buffer rings; HCI: temperature difference between BGI object border and HCDmax	HCDmean: 570 m HCDmax: 1610 m HCImean: 2.63 °C HCImax: 9.35 °C	Curve fitting and Pearson correlation coefficient	Area, LSI, percentage of vegetation, percentage of water body	**Area** (+) **LSI** (+) **Percentage of water body inside the green space** (+)
Cao et al. [205]	ASTER	90 m	TES	10-07-2000, 30-10-2003, 25-05-2004	Nagoya, Japan	Urban parks (92)	HCI: difference in temperature inside the park and the average temperature in the buffer 500 m from the park	HCImax: 6.82 °C; HCImean: 1.3 °C	Multivariate regression	Area, LSI, grass area. water area, shrubs area	**Area** (+) **Grass area** (-) **LSI** (-)
Lin et al. [138]	Landsat 5 TM	35 m from 120 m	MW	daytime; 2009-09-22	Beijing, China	Green areas (NDVI reclassification) (30)	HCD, HCI and cooling area (CA): based on watershed algorithm geometry	HCDmax: 840 m HCImean: 2.3-4.8 °C CAmax: 10.09 km2	Nonlinear regression T-student's test	Area	**Area** HCD (+) HCI (+) CA (++)
Zhao et al. [206]	Landsat 8 TIRS and MODIS-Terra	Landsat 8: 30 m MODIS: 250 m	–	2015	Xiamen, China	Vegetation surfaces	Average temperature reduction (T-air) Hourly heat absorption (MJ/a)	1.28 °C 2.04×10^9 MJ/a	–	Vegetation type	**Needleleaf forest, broadleaf forest, and mixed forest** (+)

 doi:10.20944/preprints202411.1459.v1

Nasar-u-Minallah et al. [160]	Landsat 8 TIRS and Landsat 5 TM	30 m from 100/120 m	–	2000, 2010, 2020	Lahore, Pakistan	Urban green spaces and impervious surfaces (built-up areas)	LST reduction	3 °C	Correlation analysis	Percentage of the landscape (PLAND), patch density (PD), class area (CA), largest patch index (LPI), number of patches (NP), aggregation index (AI), LSI, patch richness (PR), and mean patch shape index (SHAPE_MN)	**Aggregation of patches** (++) **PLAND** (+) **CA** (+) **LPI** (+) **Size** (+) **Shape complexity** (+)
Verma et al. [68]	Landsat 8 TIRS; PlanetScope	3 m from 100 m (downscaled via PlanetScope NDVI)	RTE/SW	16-04-2020	Lucknow, India	Urban parks	R2 of LST and BGI features in 3/6/30/60 m buffers function	HCI: 2.55 °C HCD: 18 m	Regression analysis	Area, core area index (CAI), related circumscribing circle (CIRCLE), contiguity index (CONTIG), core area (CORE), euclidean nearest neighbour distance (ENN), FRAC, radius of gyration (GYRATE), number of core areas (NCORE), PARA, patch perimeter (PERIM), shape index (SHAPE)	**CONTIG** (+) **CAI** (+) **FRAC** (+) **PARA** (+)

5.2. UCI Studies Based on Numerical Simulations

The most effective approach for modeling the cooling potential of BGI is CFD models due to their ability to simulate dynamic changes in system elements [106]. CFD produces quantitative predictions of fluid-flow phenomena based on the conservation laws (conservation of mass, momentum, and energy) governing fluid motion [105]. CFD models are based on interactions between urban fabric elements and local atmospheric parameters. These simulations account for shortwave and longwave radiation influx and outflux, anthropogenic heat, energy storage in artificial materials, evaporation, and heat exchange and transport by wind [207]. CFD results differ from remote sensing studies mainly due to limited computational capacity, which hinders comprehensive

 doi:10.20944/preprints202411.1459.v1

study of large-scale characteristics like surface area, shape complexity, and the spatial configuration of larger BGI areas. Numerical simulations usually focus on smaller-scale BGI elements like tree groves, lawns, or green roofs and walls.

One of the most effective CFD models for BGI analysis is ENVI-met, designed to simulate surface-plant-air interactions in urban environments [106, 110, 208, 209] and daily climate cycles [209]. It is a three-dimensional microclimate model based on a voxel-grid, using Reynolds Averaged Navier-Stokes equations for wind flow and an indexed view sphere scheme for radiative fluxes [106]. The simulation requires two input files: one defining area layout (buildings, vegetation, soil) and another with meteorological settings and output parameters. Newer ENVI-met generations allow defining thermal mass and heat inertia on buildings, as well as temporal variations in T-air and relative humidity [209,210].

Despite its advancements, ENVI-met still has some limitations. These include issues with radiation flux calculations, turbulence modeling which tends to overestimate the turbulent production in high acceleration areas, the grid generation, lack of information about near-wall phenomena, the inability to fully account for atmospheric flow characteristics, and the assumption of constant cloudiness and wind conditions [106,211–214].

An alternative to the commercial ENVI-met software is Ladybug Tools, which integrates its modules Butterfly and Honeybee. Butterfly is a plugin for Grasshopper/Dynamo and a Python library based on an object-oriented paradigm. It is built on OpenFOAM, an open-source CFD engine capable of running simulations and turbulence models, from simple RAS (Reynolds-Averaged Simulation) models to more complex LES (Large Eddy Simulation) models [215,216]. Honeybee, on the other hand, supports detailed daylighting and thermodynamics modeling, also being an open Python library. It allows the creation, execution, and visualization of daylighting and radiation simulations using the Radiance engine, as well as energy simulations with EnergyPlus/OpenStudio [215,216].

5.2.1. Methods for Creating BGI Representation

Both OpenFOAM and the Simple Plant Module of ENVI-met use statistical methods to describe vegetation morphology through LAI [107]. ENVI-met also includes a 3D-Plant module, which creates representations of canopy geometry as a mesh that approximates the shape and location of objects, incorporating Leaf Area Density (LAD) and Root Area Density [217]. In addition to aerodynamic characteristics, vegetation has radiation effects, described by transparency that influences the transmission of solar radiation [106–108]. Water bodies are often represented by a specific soil type, partially transparent to shortwave radiation [218], with defined heat conductivity, heat capacity, and depth. Computational processes within the water body model consider the transmission and absorption of shortwave radiation [218]. However, no secondary energy balance or supplementary boundary conditions are applied to the water or ground surfaces. As such, water grids are assumed to be deep enough to absorb most of the shortwave radiation. Some models, like ENVI-met 4.0, also simulate water spray effects, enabling the modeling of fountains and cooling through air-water aerosols [219].

5.2.2. Methods for Assessing the Cooling Potential of BGI

Analyses based on Computational Fluid Dynamics often involve comparing spatial development scenarios in terms of mean T-air or thermal comfort indices for the study area in both baseline and post-BGI implementation conditions, focusing on features such as spatial layout, coverage configuration, and tree density [220–224]. Studies assessing the maximum cooling range are rare [223], and evaluations of the area directly affected by BGI's cooling capacity are not typically performed.

In addition to T-air, CFD-based studies can also assess variations in mean radiant temperature (T-mrt), LST [182, 210, 225, 226, 227, 228], and Human Thermal Comfort Indices, such as the physiological equivalent temperature (PET) index [210], which depends on T-air, humidity, wind speed, radiation fluxes, and individual factors like body energy balance, gender, age, weight, and clothing [222]. Another example is the Universal Thermal Climate Index (UTCI), which provides an

 doi:10.20944/preprints202411.1459.v1

equivalent temperature incorporating T-air, wind speed, humidity, T-mrt, and typical clothing based on weather conditions [229].

5.2.3. Data Used for ENVI-Met Simulation

In ENVI-met, the spatial configuration file must include information on the location, dimensions, and materials of building walls and roofs. Additionally, details about vegetation, surface characteristics, and soil properties in undeveloped areas are required. Spatial parameters can be obtained through remote sensing, significantly reducing field data collection time. High spatial and spectral resolution remote sensing data are needed to ensure model accuracy. The model also requires meteorological parameters such as wind speed and direction, relative humidity, and surface roughness to initialize the simulation [230]. Table 2 presents the main input parameters required by ENVI-met along with potential data sources.

Table 2. Basic data required to run the ENVI-met model along with data source examples. Based on Heldens et al. [231].

Input data	Input parameter	Source type	Source examples
Buildings	Location	Remote sensing, cadaster maps, topographic data	PlanetScope, WorldView, QuickBird, IKONOS, ALS point clouds, airborne images, Open Street Map
	Roof material	Remote sensing (hyperspectral)	Airborne hyperspectral imagery (e.g. HyMap)
	Height	Remote sensing, photogrammetry	ALS point clouds, stereo imagery
	Material properties: reflectance properties	Remote sensing (hyperspectral)	Airborne hyperspectral imagery (e.g. HyMap)
	Material properties: thermal inertia	Literature	–
Vegetation	Location	Remote sensing	PlanetScope, WorldView, QuickBird, IKONOS, airborne images, ALS point clouds
	Type (deciduous, coniferous, grass)	Remote sensing	Airborne hyperspectral imagery (e.g. HyMap); PlanetScope, WorldView, QuickBird, IKONOS—only using time-series
	Height	Remote sensing, photogrammetry	ALS DEMs, stereo imagery
	Leaf area density	Remote sensing	Sentinel-2A integrated with ALS DEMs, Airborne hyperspectral imagery (e.g. HyMap)
	Photosynthetic and evapotranspiration properties	Literature	–
Non-build surfaces	Location	Remote sensing	PlanetScope, WorldView, QuickBird, IKONOS, airborne images
	Type (impervious, pervious)	Remote sensing	PlanetScope, WorldView, QuickBird, IKONOS, airborne images, Airborne hyperspectral imagery (e.g. HyMap)
	Soil properties (hydrological)	Literature	–
Weather conditions	Temperature, relative humidity	Weather station / field measurements	OpenSenseMap, Luftdaten, ERA5
	Wind speed and direction	Weather station / field measurements	OpenSenseMap, Luftdaten, ERA5, Global Wind Atlas
	Date, sun dawn time, sun set time	Location-related variable	–

Examples of research results on BGI characteristics influencing its cooling potential using numerical simulations are presented in Table 3.

Table 3. Examples of studies on BGI characteristics influencing its cooling efficiency using numerical simulations (+ and - indicate the direction of the feature's influence on cooling potential; the multiplicity of the sign indicates the relative significance of the influence).

 doi:10.20944/preprints202411.1459.v1

Source	Model	Study region	Time of simulation	BGI type	Cooling potential index	Cooling potential values	Method for impact assessment	BGI characteristics studied	BGI most efficient characteristics
Vidrih and Medeved [232]	Three-dimensional CFD modelling	Ljubljana, Slovenia	07-2013	Urban park	T-air	4.7 °C	Comparing different scenarios	Tree density (LAI), size	**Tree density** (+)
Skelhorn et al. [182]	ENVI-met	Manchester, UK	13-07-2014	Vegetation, mature trees and new trees	T-air	0-1 °C	Comparing different scenarios	Vegetation fraction, type (mature trees, grassland, hedge, green roof)	**Mature tree canopies area fraction** (5% → 1 °C peak LST) (+) **Hedges fraction** (5% → 0.46 °C peak LST) (+) **Green roof area fraction** (+/-)
Taleghani et al. [226]	ENVI-met	Los Angeles, USA	(30-31)-07-2014	Street trees, green roofs	T-air, T-mrt, PET	0.2 °C T-air	Comparing 6 different scenarios	Type (green roof, street trees)	**Type: street trees** (+)
Ghaffarianhoseini et al. [233]	ENVI-met	Kuala Lumpur, Malaysia	5-03-2013	Trees, grasslands	T-air	3.3 °C	Comparing different scenarios (100% grass, 25% trees, 50% trees, 75% trees)	Location and orientation, dimensions and albedo, wall enclosures, presence of greenery, type (grass, trees)	**Tree coverage** (++) **North and east orientation ofcourtyard in relation to the development** (+)
Lee et al. [210]	ENVI-met	Freiburg, Germany	04-08-2003	Trees, grasslands	PET, T-air, T-mrt	Trees: max 2.7°C T-air, 39.1 °C T-mrt, 17.4 °C PET; Grasslands: max 3.4 °C T-air, 7.5 °C T-mrt, 4.9 °C PET	Comparing different scenarios	Different types of spatial arrangements of trees and lawns, type (tree, grassland)	**Type: trees** (++) **Vegetation fraction** (+)
Morakinyo et al. [225]	ENVI-met with EnergyPlus	Cairo, Egypt; Hong-Kong; Tokyo, Japan; Paris, France	–	Green wall, green roof	Indoor T-air, LST	1.4 °C indoor T-air; 14, 10, 8.5, 7 °C LST	Comparing 60 different scenarios	4 types of green roofs	**Green roof intensity (thickness of soil and vegetation layer)** (+)

 doi:10.20944/preprints202411.1459.v1

Middel et al. [221]	ENVI-met	Phoenix (Arizona, USA)	23-06-2011	Trees	T-air (at 2 m)	max 4.4 °C	Comparing 54 different scenarios	Tree canopies area fraction	**Tree canopies area fraction** (1% → 0.14 °C peak T-air; 10% → 2 °C peak T-air) (+)
Ziaul and Pal [228]	ENVI-met	Malda, India	–	Green roofs, green walls	T-air, LST	2.6 °C T-air	Comparing different scenarios (100% green roof; 100% green roof and green wall; 50% green roof and green wall) across different development types	Different configurations of green roofs, green walls and plantings according to different development types	**For open mid-rise and compact low-rise 100% green roof and green wall** (2.6 and 1.33 °C peak T-air) **For open low-rise 50% green roof and green wall including planting** (1.87 °C peak T-air)
Ng et al. [220]	ENVI-met	Hong Kong, China	09-05-2012	Green spaces (33 different cases)	Reduction in T-air at pedestrian level	0-1.8 °C	Comparing different scenarios	Vegetation fraction, type (trees, grassland, green roof)	**Tree canopies area fraction** (33% → 1 °C peak T-air) (++) **Type: trees** (+) **Green roof area fraction** (+/-)
Lin and Lin [234]	ENVI-met	Taipei, Taiwan	–	Urban parks (8)	T-air	max 2.72 °C	Comparing different scenarios	Different types of geometries and spatial arrangements of parks	**Area** (+) **Park number** (+) **Area of the largest park** (+) **More regular spatial arrangement** (+) **Greater diversity of parks** (+)
O'Malley et al. [56]	ENVI-met	London, UK	–	Green open spaces (trees, shrubs and grass) and	T-air	1.12-1.14 °C	Comparing 3 different scenarios	Type (vegetation, water bodies)	**Vegetation** (+) **Water bodies** (+)

 doi:10.20944/preprints202411.1459.v1

				water bodies					
Santamouris et al. [235]	ENVI-met with EnergyPlus	Sydney, Australia	–	Green pavements, green roofs	T-air, energy conservation (%)	Green pavements: 0.3–1.4 °C T-air; 0.48-2.31% Energy conservation; Green roofs: 0.5 °C T-air	Comparing 3 different mitigation strategies (20, 40, 60% vegetation fraction)	Green pavement fraction; green roofs fraction	**Green pavement fraction** (20% → 0.3 °C peak T-air; 60% → 1.4 °C peak T-air) (+)
Wang et al. [222]	ENVI-met	Toronto, Canada	15-01-2013 and 15-07-2013	Urban vegetation	T-air, T-mrt	max 0.8 °C T-air	Comparing different scenarios	Urban vegetation fraction within 3 types of built-up areas	**Urban vegetation area fraction** (10% → 0.8 °C peak T-air, 8.3 °C peak T-mrt) (+)
Declet-Barreto et al. [227]	ENVI-met	Phoenix, USA	(16-17)-07-2005	Trees and grass	T-air, LST	0.9-1.9 °C T-air; 0.8-8.4 °C LST	Comparing baseline and green scenario	Greenery fraction	**Greenery fraction** (+)
Salata et al. [236]	ENVI-met	Rome, Italy	16-07-2014	Green open spaces	T-air, Mediterranean Outdoor Comfort Index (MOCI)	1.34 °C T-air; 2.5-3.5 MOCI	Comparing 6 different scenarios	Increase in vegetation fraction by 9%	**Vegetation fraction** (+)
Herath et al. [224]	ENVI-met	Colombo, Sri Lanka	(29-30)-08-2016	Green roof, green wall	T-air	Green roof: 1.76-1.9 °C	Comparing 6 different scenarios (trees in curbsides, green roofing 100%/50%, green walls 50%, combined)	Type (green roofs, green walls, trees in curbsides)	**Combined types (trees, 50% green roofs, 50% green walls)** (+++) **50% green walls** (++) **100% green roofs** (+)
Zhao et al. [125]	ENVI-met	Tempe, USA	13-06-2017	Trees	T-air, PET, wind speed	0.19 °C T-air 0.9 °C PET	Comparing 9 different scenarios	Tree density/ layout	**Equal interval trees layout (with effective ventilation)** T-air: (++) Wind speed: (+/-) **Overlapping clustered trees layout** T-air: (+) Wind speed: (-) **No trees** T-air (-) Wind speed: (++)
Cao et al. [152]	ENVI-met	Beijing, China	31-07-2018	Urban water bodies	T-air all-day cooling effect	1.57 °C	Comparing different scenarios	Water fraction, separation	**Water fraction**

 doi:10.20944/preprints202411.1459.v1

								index (SI), LSI, waterfront green space type	(64% → max cooling) (+) **LSI** (+) **SI (threshold)** (+) **GI type: trees** (+)
Berardi et al. [223]	ENVI-met, WRF-UCM	Toronto, Canada	(3-5)-07-2018	Green roofs, trees	HCI, HCD (T-air); HTCI	ENVI-met: HCI: 0.5–1.4 °C HCD: 250 m HTCI: 0.3–1.2 °C maxHTCI: 11 °C WRF-UCM: HCI: 0.8–2 °C	Comparing 2 different scenarios (50, 80%)	Green roof fraction, LAD, leaf shortwave transmittance, spatial arrangement of trees	**Vegetation fraction** (++) **LAD** (++) **Leaf shortwave transmittance** (++) **Planting trees along street canyons located parallel to the wind direction** (+)
Mohammed et al. [237]	WRF with SLUCM	Dubai, UAE	(01,07)-2019	GI	Ambient temperature	1.7 °C	Comparing different scenarios (25, 50, 75, 100%)	Greenery fraction	**Greenery fraction** (+)
Sharma et al. [238]	WRF with SLUCM	Chicago Metropolitan Area, USA	(16-18)-08-2013	Green roofs	LST	3.41 °C for roofs; ~7 °C for core urban area	Comparing different scenarios (25, 50, 75, 100%)	Green roof fraction	**Green roof fraction** (+)
Khan et al. [239]	WRF with SLUCM	Kolkata, India	(6-8)-04-2020	Green roofs	Ambient temperature	0.9 °C	Comparing different scenarios (25, 50, 75, 100%)	Green roof fraction	**Green roof fraction** (+)
Haddad et al. [240]	WRF	Riyadh, Saudi Arabia	2016-2020	Irrigated/non-irrigated GI	Ambient temperature	Irrigated: 2.1 °C; Non-irrigated: 0.8 °C	Comparing different scenarios (20-60% irrigated/non-irrigated)	Greenery fraction, irrigation	**Greenery fraction** (+) **Irrigation** (+)
Khan et al. [241]	WRF	Athens, Greece	–	GI	T-air	0.7-1.1 °C	Comparing 3 different scenarios (30, 50, 70%)	Greenery fraction	**Greenery fraction** (+)

5.3. UCI Studies Based on Field Measurements

In field measurements of UCI, the evaluation of cooling effects can be performed through T-air and other atmospheric parameters measurements, either stationary or using mobile sensors. Typically, characteristics like LAI, vegetation height, and crown density are examined in relation to meteorological conditions and their bioclimatic impact [242]. Less frequently, the size of the BGI area or the proportion of tall greenery is examined [243]. However, due to the need to make measurements at individual points, these methods usually focus on a micro or local scale, typically

 doi:10.20944/preprints202411.1459.v1

involving only a few BGI objects [244]. Nevertheless, studies based on manual measurements allow for vertical T-air profile analysis, which improves the method's value over remote sensing, allowing for inferences about the causes of advection heat exchange between BGI and urban areas.

In field studies, the most commonly measured parameter is T-air, with PET being less frequent. Common UCI measurement methods include: (1) comparing the average temperature inside a BGI element with the surrounding temperature [34] and (2) creating "cross-sections" through the BGI object and its surroundings from measurement points (mobile traverse/transect method) and evaluating the resulting function [33,244,245]. The second method uses mobile temperature loggers with GPS mounted on various vehicles, including bicycles [33]. This method allows for multiple measurements with a single device in a short period, reducing sensor installation costs while ensuring measurement homogeneity. Calibration of results based on temporal changes of the measured parameters is necessary using the optimized reentry-transect method [244]. To maintain measurement point simultaneity, transects should be created with no more than a 2-hour time gap. Often, multiple sensors are mounted on one vehicle to increase measurement frequency and accuracy. In addition to T-air, other parameters such as black globe temperature, relative humidity, wind speed, wind direction, and solar radiation are also measured [244].

Examples of research results on the features of BGI affecting its cooling potential using field measurements are presented in Table 4.

Table 4. Examples of studies on the features of BGI affecting its cooling efficiency conducted using field measurements (+ and - indicate the direction of the feature's influence on cooling potential; the multiplicity of the sign indicates the relative significance of the influence).

Source	Study region	Time of measurements	BGI type	Cooling potential index	Cooling potential values	Method of impact assessment	BGI characteristics studied	BGI most efficient characteristics
Vaz Monteiro et al. [243]	London, UK	20-06-2012 to 2-10-2012 (nocturnal cooling)	Green open spaces and tree canopy	Reduction of LST; HCD	0.6-1 °C LST; HCD: 100-150 m	Temperature measurements at different distances from the BGI	Area, PARA, Tree coverage, grass coverage	**Area** (++) **Tree coverage** (+) **Grass coverage** (+)
Spronken-Smith et al. [33]	Vancouver, BC and Sacramento,CA	(07-08)-1992 (Vancouver); 08-1993 (Sacramento)	Green open spaces	Reduction of T-air and LST	max 6.5 °C T-air; average (day): 2.4 °C average (night): 3.3 °C	Temperature measurements at different distances from the BGI (bicycle traverse)	Type (grass, grass with tree border, savannah, golf course, garde, multiuse, forest), tree coverage, irrigation	**Tree coverage** (++) **Type: sparsely treed savannah park in a semi rural settings** (+) **Irrigation** (+)
Chang et al. [34]	Taipei, Taiwan	(08-09)-2003; from 12-2003 to 01-2004	Urban parks (61)	Reduction of T-air	mean: 0.59 °C max: 1.51 °C	T-air measurements at 2 m: inside the park and in the surroundings	Area, tree and shrub coverage, turf coverage, tree coverage	**Area (<3 ha)** (++) **Tree coverage** (+)
Cohen et al. [74]	Tel Aviv, Israel	2007-2011	Parks, squares, street canyons	Reduction of T-air and PET	2-4.5 °C T-air 10-18 °C PET	Measurements by fixed meteorological stations	BGI type, BGI layout, tree coverage	**Tree coverage** (++) **Deciduous trees type** (+)
Hoellscher et al. [246]	Berlin, Germany	16-07-2013	Green facade	Reduction of T-air/LST	15.5 °C LST	Temperature comparison between a green wall and a standard building façade	Different plant species, various arrangements of vegetation on façades	**Design of facade greenery** (+) LST (+/-) T-air
Hamada and Ohta [247]	Nagoya, Japan	08-2006 to 07-2007	Urban park	Reduction of T-air; HCD	0.3-1.9 °C T-air	Measurements by fixed	Forest cover ratio	**Forest cover ratio** (+)

 doi:10.20944/preprints202411.1459.v1

		HCD: 200-300 m	meteorological stations

6. Technologies with the Potential to Develop Tools to Optimize BGI Planning and Management

In spatial planning, BGI is one of the most effective tools for mitigating and adapting to climate change. Adaptation, in addition to reducing thermal stress, includes alleviating the intensity of flash floods [248], enhancing resilience to urban droughts [249], air purification [250], and increasing biodiversity [251]. Mitigation using BGI mainly involves carbon dioxide sequestration [19] and energy consumption reduction [252]. Optimal BGI implementation requires considering the relationships between all potential outcomes, not just urban thermal issues, ensuring that the solutions are as effective as possible overall. Given the complexity of the problem, tools based solely on numerical simulations, remote sensing, and other measurements become insufficient. In this context, more complex systems and technologies are necessary, such as Digital Twin (DT). DT is defined as "a virtual representation of a physical system (and its associated environment and processes) that is updated through the exchange of information between the physical and virtual systems" [253]. A key element of DT is ensuring connectivity between the model and the real world. DT is closely linked with Artificial Intelligence (AI), Big Data (BD), Internet of Things (IoT), and edge processing for data collection and processing, enabling real-time system monitoring as well as simulating changes under specific parameter modification scenarios. Although the term DT was first mentioned in the early 21st century, it has only become widespread in cities in recent years, thanks to the development of digital infrastructure and data-based technologies [254], becoming an integral part of the smart city concept [254,255].

Urban DTs are used for power grids, energy demand, renewable energy, mobility, public transportation, road infrastructure, water supply, sewage, noise pollution, flooding, and climatology [254–257]. Most research focuses on their conceptualization or application within narrow industry frameworks [253,255,258–260]. However, there is limited knowledge on creation and implementation of comprehensive DTs. In the context of BGI, despite the enormous potential and developmental capabilities of DT technology, no comprehensive system has yet been implemented for its planning and management at the urban scale, considering all ecosystem services and the level of detail needed for local planning.

DT technology for BGI planning and management should encapsulate data on key processes in urban environments across various scales. Ensuring interoperability between systems is crucial for effective information exchange and better decision-making through more accurate forecasting. A promising approach is AI for managing IoT (AIoT) [261]. Current interoperability challenges include data silos from infrastructure providers [262], isolation in public sectors [263], and tight coupling of data to specific applications [257,264], along with the complexity of multiple scales and domains [265]. Additionally, data heterogeneity in scale, detail, accuracy, and spatial and temporal uniformity, combined with BGI's complex relationships with urban space, makes defining semantic rules for dynamic city representation difficult [266,267]. Therefore, creating new metadata standards and universal data exchange formats is necessary for effective data fusion [254,268,269].

Infrastructure is crucial, including computing, networks, and data storage [254]. DT technologies, such as IoT [270] and increasingly detailed 3D models with Augmented Reality (AR) [271], require highly efficient real-time data processing [270]. This necessitates the development of new data processing engines [272] or edge computing architectures [273], along with higher-capacity networks. Beyond processing, data storage and archiving vast amounts of data used by DT become critical [264]. A promising direction is the development of efficient decentralized data storage architectures [273]. A key issue is also data acquisition [254]. Current IoT networks (e.g., Open Sense Map) may be too fragmented and heterogeneous to maintain proper temporal and spatial continuity [264]. Further challenges include synchronizing real-time measurement frequencies [255], network speed, and connectivity continuity. Synchronization affects data generation, distribution, and analysis speed, which is crucial for real-time processing [254]. Additionally, despite the existence of various IoT networks, some environmental, social, or economic data are still

 doi:10.20944/preprints202411.1459.v1

missing, and some lack sufficient quality and reliability to ensure the accuracy and realism of DT [264, 274, 275].

A key challenge is ensuring an optimal modeling and simulation system for evaluating urban development scenarios. This is crucial for improving decision-support systems [254]. Promising advancements in machine learning and deep learning (ML/DL) are being explored for processing data in DT [275]. However, challenges remain with computational limitations, integrating models at multiple scales, ensuring data quality [272,273], and managing the complexity of urban systems [276], along with the lack of sufficient validation [264], uncertainty quantification [277], and adaptation to extreme situations [266]. Maintaining informative visualizations of results is also essential, with potential in technologies such as AR, Extended (XR), Virtual (VR), and Mixed Reality (MR) [254].

Beyond technological challenges, the development and implementation of DT for BGI may be hindered by the need for a skilled workforce and funding to develop and maintain the infrastructure [254]. Additionally, the diverse and dispersed nature of BGI may require various sub-models to accurately simulate elements like water, vegetation, soil, heat exchange, or flood risk. Despite these challenges, implementing DT technology in cities can significantly improve the efficiency of decision-making processes related to BGI planning and management [278]. Research focused on the development of DT for BGI should therefore be a priority in optimizing planning and management methods, both in conceptualization and in the construction and integration of specific geoinformatics products and spatial data to support the creation of more resilient cities.

7. Discussion

7.1. Interpretation and Findings

7.1.1. Differences Between Results Obtained Using Different Approaches

Each approach to assessing cooling potential—remote sensing, numerical simulations, and field measurements—offer unique capabilities for analyzing BGI [110]. Numerical simulations require the most data and significant computational power, even for analyzing small areas [42]. Remote sensing methods, on the other hand, can often rely on readily available products covering thousands of square kilometers [43]. However, remote sensing is limited to measuring LST within the sensor's specific angle, restricting information about urban thermal conditions, especially in areas with complex morphology [51]. Field measurements require minimal data, have a high temporal resolution and are suitable for analyzing short-term trends, but are limited by the accessibility of certain urban locations, such as private properties [279].

The research objective and scale of analysis are key in selecting the appropriate method. At the local scale, if the goal is to assess BGI characteristics relevant to urban planning (e.g., BGI area geometry, vegetation density, and urban morphology impact), remote sensing is the best choice. It captures broad spatial context, allowing analysis of multiple large BGI areas simultaneously, though it is effective only for evaluating existing BGI features. At the neighborhood scale, when evaluating the effectiveness of different BGI development scenarios, numerical simulations are optimal. This method supports micro-scale analysis, such as assessing solutions like green roofs and walls. Field measurements, on the other hand, excel in capturing actual atmospheric parameters necessary for calculating thermal comfort indices, providing insight into BGI's real impact on urban livability.

Aside from diverse urban morphology and meteorological and climatic conditions, variations in results may stem from differing definitions of BGI cooling effectiveness. For remote sensing studies, comparisons typically involve contrasting LST values within or at the edge of a BGI feature with those of the immediate surroundings, e.g., [66]. Field measurements use the same method but focusing on T-air differences, e.g., [33]. In numerical simulations, cooling effectiveness is often reflected by differences in average T-air across the study area before and after introducing specific BGI configurations, e.g., [221]. The latter approach simulates BGI's potential impact on urban

 doi:10.20944/preprints202411.1459.v1

temperature reduction, offering insights into cooling effectiveness, though the results inherently carry some uncertainty.

LST resolution notably impacts results in estimations using remote sensing. Studies using lower-resolution data report broader cooling extents than those based on high-resolution LST [68], indicating that "mixed pixels" might artificially expand cooling zones. This effect is particularly evident with common Landsat 8/9 data, which use TIRS images with a native 100 m resolution, downscaled to 30 m. Each 100 m pixel averages diverse urban surfaces, thus blurring BGI boundaries and potentially intensifying the gradient effect of rising LST with distance from the BGI site. Additionally, the land use around the BGI can reinforce the LST gradient effect if smaller vegetation structures, like single trees or green roofs, reflect a gradient of decreasing vegetation density with distance. Building configurations that cast shadows also influence localized LST values, potentially lowering pixel readings. These challenges become less pronounced with higher-resolution imagery. Downscaled images, however, may introduce errors associated with the statistical resolution enhancement. Results may also vary due to cooling potential calculation methods, including buffer widths and other methods used.

Another important factor affecting results is the method of BGI delimitation. Using BGI boundaries from urban databases often overlooks the actual extent of vegetation in favor of property boundaries. Such approach is highly susceptible to errors caused by the surrounding morphology impacting cooling zone anomalies. More effective methods involve processing remote sensing imagery (e.g., image classification or vegetation index reclassification [66]), allowing for objective, uniform delineation of BGI's physical boundaries. It is important to use the same imagery source for both LST calculations and BGI delimitation (e.g., Landsat 8/9—OLI bands for BGI delimitation and TIRS bands for LST calculations), minimizing errors due to georeferencing or radiometric corrections.

In numerical simulations, we confirmed that the largest discrepancies occur between micro- and mesoscale models [42]. This is primarily because models at different scales apply distinct assumptions regarding physical heat exchange processes in urban spaces. Mesoscale models often simplify local phenomena, such as the cooling effect of individual trees or small green spaces, and cannot fully describe heat fluxes in urban canyons [110]. Conversely, microscale models offer more detail and can better represent these localized processes, yet they are limited in generalizing results across larger areas.

Significant differences can also be observed among models at the same scale, despite simulating identical scenarios and conditions. This variability often results from differences in how models implement and parameterize physical processes related to BGI's cooling mechanisms in urban spaces. Models may vary in their representation of vertical heat transport or surface-atmosphere energy exchanges, which impacts outcomes.

Furthermore, a model's ability to accurately recreate the microclimatic conditions of a specific area does not ensure its suitability for simulating BGI cooling potential. Cooling effects from evapotranspiration and shading require specific sub-models, which are not typically assessed in standard numerical simulation tests. Thus, for UCI studies, model physics evaluation should be conducted with stricter criteria to enhance the reliability of simulation results [42].

In field-based studies, differences in results may arise from how microclimatic factors are recorded, such as how sensors are shielded from solar radiation. Variations can also stem from the method of data collection itself. Results can differ between studies based on data from fixed monitoring stations and those using mobile recorders, as the latter may be more precise [110]. Additionally, differences may arise from time shifts in measurements when using mobile traverse methods. It is evident that without accounting for changes in T-air over the daily cycle, measurements taken along a transect from the studied BGI object outward may show an increasing trend, even if the object itself does not exhibit cooling properties. Therefore, the use of the optimized reentry-transect method is necessary [244].

7.1.2. BGI Characteristics Affecting Cooling Potential

 doi:10.20944/preprints202411.1459.v1

BGI is an effective tool for mitigating both LST and T-air, improving thermal comfort and enhancing the quality of urban life and energy efficiency. In LST-based studies, the most commonly analyzed BGI characteristics impacting cooling efficiency include geometry (area, perimeter, LSI, and other perimeter/surface ratios), canopy cover, and surface water fraction [41, 59, 62, 166, 183]. Numerical simulation studies often focus on vegetation fraction and various BGI configurations (including trees and green roofs) [210, 220, 221, 237, 241]. Field measurement studies typically examine BGI surface area and the proportion of tall vegetation [33, 34, 243, 247]. In all cases, the most important feature is the BGI area. Most studies have shown that larger BGI objects (defined as vegetation-covered areas) cool urban spaces more intensively and over a larger scale [138, 203, 204, 205]. However, the cooling capacity increase is not proportional to the increase in BGI area. Studies suggest the need to identify the minimum area that ensures effective cooling [55], balancing economic viability and efficient space use. Besides the BGI scale, vegetation intensity and quality are essential. In remote sensing, NDVI [62, 158] or LAI can define this characteristic; in numerical simulations, LAI, LAD, or vegetation type diversity level [223, 224, 232]; and in field measurements, the proportion of tall vegetation [33, 34, 243, 247]. However, adequate ventilation is also crucial, so vegetation should not be overly dense [125].

Additionally, specific characteristics that can only be assessed using a single method type can be distinguished. For example, comparing the cooling efficiency of green walls and roofs to traditional BGI is feasible only through numerical simulations. Although green roofs help regulate local temperatures, they are less effective than conventional BGI [182, 220, 226], limiting their cost-effectiveness to dense urban settings where creating ground-level BGI is not feasible. Another group of BGI characteristics are landscape metrics, which can only be assessed through remote sensing. In this context, the most important factor is the spatial connection of BGI [68,160].

The complexity of BGI shapes is often studied, but the results are inconsistent. The differences may stem from varying locations and climatic characteristics of the studied areas [143, 166, 280], and different interpretations of statistical analysis results. Commonly studied indicators like LSI often correlate strongly with shape area, leading to potential misinterpretations that larger LSI implies greater cooling. An additional source of uncertainty may be the varied urban morphology, which can modify the cooling potential of specific BGI shapes [72, 77, 116, 147, 148]. Therefore, when evaluating the impact of shape complexity, it is important to first confirm the lack of correlation with shape area and assess the effect of surrounding building morphology.

7.2. Gaps and future research directions

7.2.1. Incorporating factors related to urban morphology around BGI

Studies on the cooling capacity of BGI features rarely address characteristics of surrounding urban morphology, despite its potential impact on BGI's cooling ability by increasing temperature and humidity contrasts [72, 77, 116, 183, 281] and thermal stress on vegetation [40,148]. Future research should place more emphasis on this aspect. The focus should be on utilizing the LCZ concept. A useful tool for remote sensing could be the World Urban Database and Access Portal Tools LCZ Generator [282], which enables semi-automatic classification of urban areas based on morphological diversity relevant to thermal dynamics.

7.2.2. Development of an objective method for delimiting BGI objects for analysis

Regardless of the adopted definition of cooling, the delimitation of BGI shapes has the greatest impact on the obtained results. Therefore, it is essential to use objective methods for delimiting BGI objects. One such method can be Geographic Object-based Image Analysis (GEOBIA) [283,284], preferably performed using the same image employed to calculate the LST data.

7.2.3. Integration of new spatial data

An important direction should be the integration of new, less-explored spatial data, such as ECOSTRESS LST. Such analyses could shed new light on the changes in the cooling potential of BGI

 doi:10.20944/preprints202411.1459.v1

over a 24-hour cycle, including at night, which would be important, for example, in assessing the impact of BI on nocturnal SUHI. It is also necessary to aim for higher-resolution LST data [166] and greater engagement of IoT, which could assist in both better validation of CFD studies and the accuracy of T-air estimations from LST using geostatistical techniques. Additionally, UAV measurements [285] offer promising potential for validating simulations and providing precise thermal data, especially for surfaces inaccessible by standard remote sensing, enabling more accurate assessments of BGI characteristics.

7.2.4. Research on a large scale or the integration of results into a universal indicator

Different climates and geographic locations can significantly impact the results of BGI's cooling potential. An objective assessment of BGI characteristics requires analyzing cases from various contexts. To achieve this, studies should be expanded based on automated analytical procedures that allow for the simultaneous analysis of multiple cities using a unified method (e.g., [286]), or through literature reviews that incorporate the standardization of results, e.g., [42].

7.2.5. Correct interpretation of results obtained using LST

The results of remote sensing analyses do not represent perceived temperature but rather LST, influenced by emissivity and other physical parameters of different surface configurations. BGI affects LST primarily through shading and evapotranspiration, which is well documented. However, the cooling mechanisms of LST in areas distant from BGI require further research and validation to address resolution and urban morphology issues.

7.2.6. Development of comprehensive urban ventilation models

Wind conditions modify BGI cooling capacity and thermal comfort. Effective BGI management requires detailed city-wide ventilation simulations that consider urban morphology and BGI features. However, current CFD models are scale-limited, partly due to computational constraints. Therefore, advancing CFD and related technologies with AI support (e.g., graph neural networks [287]) is essential.

7.2.7. Use of the Digital Twin technology

There is a need to unify approaches for assessing the cooling potential of BGIs and standardize data for interoperable solutions. Future BGI research should move away from traditional methodologies towards revolutionary concepts like DT. It is essential to combine AI, IoT, and BD technologies with the practical needs of implementing DT in cities for optimizing BGI planning and management. The main challenges include: (1) interoperability and semantics; (2) computational infrastructure, networks, and data storage; (3) data acquisition, synchronization, and updating; (4) data quality and harmonization; (5) modeling and simulation of real phenomena, and integration with decision-making systems; (6) visualization informativeness; (7) human and financial resources; (8) legislative, organizational, and social issues [254]. These topics require the most attention in future research to enable the creation and implementation of holistic tools for optimizing BGI planning and management to enhance cities' resilience to climate change.

8. Conclusions

This study aimed to systematize knowledge through a literature review on using geoinformatics tools and spatial data to assess BGI cooling potential for spatial planning optimization. The objectives were to: (1) explain the mechanisms behind BGI cooling, (2) discuss effective BGI features, (3) analyze the impact of spatial data and methods on results, and (4) suggest future research directions.

BGI cooling mainly comes from vegetation's evapotranspiration, shading, and wind flow modification, which enable evapotranspiration and convective cooling. The surrounding urban morphology also affects cooling through further modifying the park-breeze effect and thermal stress on vegetation. Key BGI features enhancing cooling efficiency include size, vegetation density, height,

multi-level structure, and spatial configuration. Green roofs and walls are less effective than traditional BGI types. It remains unclear whether the shape complexity positively influences the cooling ability of BGI in every morphological context.

Methods such as remote sensing, numerical simulations, and field measurements vary in analytical capabilities, which differentiates their effectiveness to fulfill specific research needs. The remote sensing approach compares LST inside and around BGI, numerical simulations analyze mean temperature changes before and after BGI implementation, and field measurements focus on T-air differences within specific locations. Results vary mainly due to geographical and climatic differences, as well as in reference to cooling efficiency definitions, data resolution, BGI delimitation methods, and the types of simulation models used. Remote sensing analyses tend to overestimate cooling effects, especially with low-resolution data.

Key research gaps include deepening the understanding of the urban morphology's impact on the modification of BGI cooling effects and integrating new spatial data, including night-time and UAV LST, and meteorological data from IoT. A promising research direction is the development of Digital Twin technology for BGI planning and management optimization. However, challenges remain in implementing this technology, including data and model semantics, data quality, and real-time simulations.

Author Contributions: Conceptualization: G.B.; Data curation: G.B.; Formal analysis: G.B.; Investigation: G.B.; Methodology: G.B.; Project administration: T.K.; Resources: G.B.; Software: G.B.; Supervision: T.K.; Validation: G.B.; Visualization: G.B.; Writing - original draft: G.B., M.S.; Writing - review & editing: M.S., T.K.

Funding: This work was supported by the Ministry of Science and Higher Education (Poland).

Data Availability Statement: No new data were created or analyzed in this study. Data sharing is not applicable to this article.

Conflicts of Interest: The authors declare no conflicts of interest.

Reference

1. Easterling, D. R. et al. Climate Extremes: Observations, Modeling, and Impacts. Science 2000, 289. https://doi.org/10.1126/science.289.5487.2068
2. Stephenson, D. Definition, diagnosis, and origin of extreme weather and climate events;, 2008. https://doi.org/10.1017/CBO9780511535840.003.
3. Meehl, G.A. and Tebaldi, C. More Intense, More Frequent, and Longer Lasting Heat Waves in the 21st Century. Science 2004, 305. https://doi.org/10.1126/science.1098704
4. Meehl, G. A. et al. An introduction to trends in extreme weather and climate events: Observations, socioeconomic impacts, terrestrial ecological impacts, and model projections. B Am Meteorol Soc. 2000, 81. https://doi.org/10.1175/1520-0477(2000)081<0413:AITTIE>2.3.CO;2
5. D'Ippoliti, D. The impact of heat waves on mortality in 9 European cities: Results from the EuroHEAT project. Environmental health: a global access science source 2010, 9. https://doi.org/10.1186/1476-069X-9-37
6. Semenza, J. C. et al. Heat-related deaths during the July 1995 heat wave in Chicago. N Engl J Med 1996, 335. https://doi.org/10.1056/NEJM199607113350203
7. Kotz, M. et al. The economic commitment of climate change. Nature 2024, 628. https://doi.org/10.1038/s41586-024-07219-0
8. Newman, R. The global costs of extreme weather that are attributable to climate change. Nature Communications 2023, 14. https://doi.org/10.1038/s41467-023-41888-1
9. Maxwell, S. et al. Conservation implications of ecological responses to extreme weather and climate events. Diversity and Distributions 2018, 25. https://doi.org/10.1111/ddi.12878
10. Garrabou, J. et al. Mass mortality in Northwestern Mediterranean rocky benthic communities: effects of the 2003 heat wave. Global Change Biology 2009, 15. https://doi.org/10.1111/j.1365-2486.2008.01823.x
11. Howard, L. The climate of London: deduced from meteorological observations made in the metropolis and at various places around it, London, 1833.
12. Sundborg, A. A. Climatological Studies in Uppsala. With Special Regard to the Temperature Conditions in the Urban Area; Appelbergs Boktryckeri Aktiebolag, Uppsala, 1951.
13. Oke, T. R. The energetic basis of urban heat island. Quarterly Journal of the Royal Meteorological Society 1982, 108. https://doi.org/10.1002/qj.49710845502

14. Oke, T. R. City size and the urban heat island. Atmospheric Environment 1973, 7. https://doi.org/10.1016/0004-6981(73)90140-6
15. Kalnay, E. and Cai, M. Impact of Urbanization and Land-Use Change on Climate. Nature 2003, 423. https://doi.org/10.1038/nature01675
16. McCarthy, M. P. et al. Climate change in cities due to global warming and urban effects. Geophysical Research Letters 2010, 37. https://doi.org/10.1029/2010GL042845
17. Bazrkar, M. H. et al. Urbanization and Climate Change; In: Leal Filho, W. (eds) Handbook of Climate Change Adaptation. Springer, Berlin, Heidelberg, 2015. https://doi.org/10.1007/978-3-642-38670-1_29
18. Qian, Y. et al. Urbanization Impact on Regional Climate and Extreme Weather: Current Understanding, Uncertainties, and Future Research Directions. Adv Atmos Sci. 2022, 39. https://doi.org/10.1007/s00376-021-1371-9
19. Intergovernmental Panel on Climate Change (IPCC). Summary for Policymakers. In: Climate Change 2021 – The Physical Science Basis: Working Group I Contribution to the Sixth Assessment Report of the Intergovernmental Panel on Climate Change; Cambridge University Press, 2023. https://doi.org/10.1017/9781009157896
20. Zhan, Y. et al. Urbanization can accelerate climate change by increasing soil N2O emission while reducing CH4 uptake. Global Change Biology 2023, 29. https://doi.org/10.1111/gcb.16652
21. Tan, J. et al. The urban heat island and its impact on heat waves and human health in Shanghai. Int J Biometeorol 2010, 54. https://doi.org/10.1007/s00484-009-0256-x
22. European Commission. COMMUNICATION FROM THE COMMISSION TO THE EUROPEAN PARLIAMENT, THE COUNCIL, THE EUROPEAN ECONOMIC AND SOCIAL COMMITTEE AND THE COMMITTEE OF THE REGIONS. Green Infrastructure (GI) – Enhancing Europe's Natural Capital 2013, 41400.
23. Givoni, B. Impact of planted areas on urban environmental quality: A review. Atmospheric Environment. Part B. Urban Atmosphere 1991, 25. https://doi.org/10.1016/0957-1272(91)90001-U
24. Gill, S. et al. Adapting Cities for Climate Change: The Role of the Green Infrastructure. Built Environment 2007, 33. https://doi.org/10.2148/benv.33.1.115
25. Monteiro, R. et al. Green Infrastructure Planning Principles: An Integrated Literature Review. Land 2020, 9. https://doi.org/10.3390/land9120525
26. Costanza, R. et al. The value of the world's ecosystem services and natural capital. Nature 1996, 387.
27. Almaaitah, T. et al. The potential of Blue-Green infrastructure as a climate change adaptation strategy: a systematic literature review. Blue-Green Systems 2021, 3. https://doi.org/10.2166/bgs.2021.016
28. Reid, W. V. et al. Millennium Ecosystem Assessment. Ecosystems and Human Well-being: synthesis; Island Press, 2005.
29. Voskamp, I.M. and Van de Ven, F. H. M. Planning support system for climate adaptation: Composing effective sets of blue-green measures to reduce urban vulnerability to extreme weather events. Building and Environment 2015, 83. https://doi.org/10.1016/j.buildenv.2014.07.018
30. Demuzere, M. et al. Mitigating and adapting to climate change: Multi-functional and multi-scale assessment of green urban infrastructure. Journal of environmental management 2014, 146. https://doi.org/10.1016/j.jenvman.2014.07.025
31. Januchta-Szostak, A. Błękitno-zielona infrastruktura jako narzędzie adaptacji miast do zmian klimatu w zagospodarowania wód opadowych. Architektura, Urbanistyka, Architektura Wnętrz 2020, 3. https://doi.org/10.21008/j.2658-2619.2020.3.3
32. Jim, C. Y. et al. Charting the green and climate-adaptive city. Landscape and Urban Planning 2015, 138. https://doi.org/10.1016/j.landurbplan.2015.03.007
33. Spronken-Smith, R.A. and Oke, T. R. The Thermal Regime of Urban Parks in Two Cities with Different Summer Climates. International Journal of Remote Sensing 1998, 19. https://doi.org/10.1080/014311698214884
34. Chang, C. R. et al. A preliminary study on the cool-island intensity of Taipei city parks. Landscape and Urban Planning 2007, 80. https://doi.org/10.1016/j.landurbplan.2006.09.005
35. Yang, X. et al. The urban cool island phenomenon in a high-rise high density city and its mechanisms. International Journal of Climatology 2017, 37. https://doi.org/10.1002/joc.4747
36. Zhao-wu, Y. U. et al. Impacts of urban cooling effect based on landscape scale: A review. Chinese Journal of Applied Ecology 2015, 26.
37. Xie, Q. et al. Regulation of water bodies to urban thermal environment: Evidence from Wuhan, China. Frontiers in Ecology and Evolution 2023, 11. https://doi.org/10.3389/fevo.2023.983567
38. Anjos, M. and Lopes, A. Urban Heat Island and Park Cool Island Intensities in the Coastal City of Aracaju, North-Eastern Brazil. Sustainability 2017, 9. https://doi.org/10.3390/su9081379
39. Ren, Z. et al. Estimation of the Relationship between Urban Park Characteristics and Park Cool Island Intensity by Remote Sensing Data and Field Measurement. Forests 2013, 4. https://doi.org/10.3390/f4040868

40. Kong, F. et al. Effects of spatial pattern of greenspace on urban cooling in a large metropolitan area of eastern China. Landscape and Urban Planning 2014, 128. https://doi.org/10.1016/j.landurbplan.2014.04.018
41. Yu, Z. et al. How can urban green spaces be planned for climate adaptation in subtropical cities? Ecological Indicators 2017, 82. https://doi.org/10.1016/j.ecolind.2017.07.002
42. Krayenhoff, E. S. et al. Cooling hot cities: A systematic and critical review of the numerical modelling literature. Environmental Research Letters 2021, 16. https://doi.org/10.1088/1748-9326/abdcf1
43. Zhou, D. et al. Satellite Remote Sensing of Surface Urban Heat Islands: Progress, Challenges, and Perspectives. Remote Sensing 2019, 11. https://doi.org/10.3390/rs11010048
44. Bahi, H. et al. Review of methods for retrieving urban heat islands. Materials Today: Proceedings 2020, 27. https://doi.org/10.1016/j.matpr.2020.03.272
45. Voogt, J.A. and Oke, T. R. Thermal remote sensing of urban climates. Remote Sensing of Environment 2003, 86. https://doi.org/10.1016/S0034-4257(03)00079-8
46. Oyler, J. W. et al. Remotely sensed land skin temperature as a spatial predictor of air temperature across the conterminous United States. Journal of Applied Meteorology and Climatology 2016, 55. https://doi.org/10.1175/JAMC-D-15-0276.1
47. Good, E. An in situ-based analysis of the relationship between land surface "skin" and screen-level air temperatures: Land Skin-Air Temperature Relationship. Journal of Geophysical Research: Atmospheres 2016, 121. https://doi.org/10.1002/2016JD025318
48. Mirzaei, P.A. and Haghighat, F. Approaches to study urban heat island–abilities and limitations. Building and environment 2010, 45. https://doi.org/10.1016/j.buildenv.2010.04.001
49. Becker, F. and Li, Z. L. Surface temperature and emissivity at various scales: Definition, measurement and related problems. Remote sensing reviews 1995, 12. https://doi.org/10.1080/02757259509532286
50. Hulley, G.C. and Ghent, D. Taking the Temperature of the Earth: Steps towards Integrated Understanding of Variability and Change; Elsevier: Amsterdam, The Netherlands, 2019.
51. Hulley, G. et al. New ECOSTRESS and MODIS Land Surface Temperature Data Reveal Fine-Scale Heat Vulnerability in Cities: A Case Study for Los Angeles County, California. Remote Sensing 2019, 11. https://doi.org/10.3390/rs11182136
52. Li, C. and Yu, C. W. Mitigation of urban heat development by cool island effect of green space and water body; Proceedings of the 8th International Symposium on Heating, Ventilation and Air Conditioning, Springer, 2014. https://doi.org/10.1007/978-3-642-39584-0_62
53. O'Malley, C. et al. Urban Heat Island (UHI) mitigating strategies: A case-based comparative analysis. Sustainable Cities and Society 2015, 19. https://doi.org/10.1016/j.scs.2015.05.009
54. Qiu, G. Y. et al. Experimental studies on the effects of green space and evapotranspiration on urban heat island in a subtropical megacity in China. Habitat International 2017, 68. https://doi.org/10.1016/j.habitatint.2017.07.009
55. Yu, Z. et al. Critical review on the cooling effect of urban blue-green space: A threshold size perspective. Urban Forestry and Urban Greening 2020, 49. https://doi.org/10.1016/j.ufug.2020.126630
56. O'Malley, C. et al. Urban Heat Island (UHI) mitigating strategies: a case-based comparative analysis. Sustainable Cities and Society 2015, 19.
57. Du, H. et al. Research on the cooling island effects of water body: A case study of Shanghai, China. Ecol. Indic. 2016, 67. https://doi.org/10.1016/j.ecolind.2016.02.040
58. Yang, G. et al. How can urban blue-green space be planned for climate adaption in high-latitude cities? A seasonal perspective. Sustainable Cities and Society 2020, 53. https://doi.org/10.1016/j.scs.2019.101932
59. Qiu, X. et al. Cooling Effect of Urban Blue and Green Spaces: A Case Study of Changsha, China. Int. J. Environ. Res. Public Health 2023, 20. https://doi.org/10.3390/ijerph20032613
60. Gao, Y. et al. Analysis of the spillover characteristics of cooling effect in an urban park: A case study in Zhengzhou city. Front. Earth Sci 2023, 11. https://doi.org/10.3389/feart.2023.1133901
61. Yao, X. et al. How can urban parks be planned to mitigate urban heat island effect in "Furnace cities"? An accumulation perspective. Journal of Cleaner Production 2022, 330. https://doi.org/10.1016/j.jclepro.2021.129852
62. Du, H. et al. Quantifying the cool island effects of urban green spaces using remote sensing data. Urban For. Urban Green 2017, 27. https://doi.org/10.1016/j.ufug.2017.06.008
63. Tan, X. et al. Comparison of cooling effect between green space and water body. Sustainable Cities and Society 2021, 67. https://doi.org/10.1016/j.scs.2021.102711
64. Liu, W. et al. Green Space Cooling Effect and Contribution to Mitigate Heat Island Effect of Surrounding Communities in Beijing Metropolitan Area. Front. Public Health 2022, 10. https://doi.org/10.3389/fpubh.2022.870403
65. Kirschner, V. et al. Measuring the relationships between various urban green spaces and local climate zones. Scientific Reports 2023, 13. https://doi.org/10.1038/s41598-023-36850-6
66. Sun, R. et al. Cooling effects of wetlands in an urban region: The case of Beijing. Ecological Indicators 2012, 20. https://doi.org/10.1016/j.ecolind.2012.02.006

67. Guo, F. et al. Study on the mechanism of urban morphology on river cooling effect in severe cold regions. Frontiers in Public Health 2023, 11. https://doi.org/10.3389/fpubh.2023.1170627
68. Verma, R. et al. The relationship between spatial configuration of urban parks and neighbourhood cooling in a humid subtropical city. Landscape Ecology 2024, 39. https://doi.org/10.1007/s10980-024-01818-y
69. Skoulika, F. et al. On the thermal characteristics and the mitigation potential of a medium size urban park in Athens, Greece. Landscape and Urban Planning 2014, 123. https://doi.org/10.1016/j.landurbplan.2013.11.002
70. Doick, K. J. et al. The role of one large greenspace in mitigating London's nocturnal urban heat island. Science of The Total Environment 2014, 493. https://doi.org/10.1016/j.scitotenv.2014.06.048
71. Ca, V. T. et al. Reductions in air conditioning energy caused by a nearby park. Energy and Buildings 1998, 29. https://doi.org/10.1016/S0378-7788(98)00032-2
72. Jansson, C. et al. Near surface climate in an urban vegetated park and its surroundings. Theor. Appl. Climatol. 2007, 89. https://doi.org/10.1007/s00704-006-0259-z
73. Lee, S. H. et al. Effect of an urban park on air temperature differences in a central business district area. Landscape and Ecological Engineering 2009, 5. https://doi.org/10.1007/s11355-009-0067-6
74. Cohen, P. et al. Daily and seasonal climatic conditions of green urban open spaces in the Mediterranean climate and their impact on human comfort. Building and Environment 2012, 51. https://doi.org/10.1016/j.buildenv.2011.11.020
75. Oke, T. R. Boundary Layer Climates; Routledge, New York, 1987.
76. Oke, T. R. The distinction between canopy and boundary-layer urban heat islands. Atmosfera 1976, 14.
77. Gunawardena, K. R. et al. Utilising green and bluespace to mitigate urban heat island intensity. Science of The Total Environment 2017, 584-585. https://doi.org/10.1016/j.scitotenv.2017.01.158
78. Nichol, J. E. et al. Urban heat island diagnosis using ASTER satellite images and 'in situ' air temperature. Atmospheric Research 2009, 94. https://doi.org/10.1016/j.atmosres.2009.06.011
79. Schwarz, N. et al. Relationship of land surface and air temperatures and its implications for quantifying urban heat island indicators—An application for the city of Leipzig (Germany). Ecological Indicators 2012, 18. https://doi.org/10.1016/j.ecolind.2012.01.001
80. Smoliak, B. V. et al. Dense Network Observations of the Twin Cities Canopy-Layer Urban Heat Island. Journal of Applied Meteorology and Climatology 2015, 54. https://doi.org/10.1175/JAMC-D-14-0239.1
81. Chen, Q. et al. Spatially explicit assessment of heat health risk by using multi-sensor remote sensing images and socioeconomic data in Yangtze River Delta, China. International Journal of Health Geographics 2018, 17. https://doi.org/10.1186/s12942-018-0135-y
82. Hussain, S. et al. Relation of land surface temperature with different vegetation indices using multi-temporal remote sensing data in Sahiwal region, Pakistan; Geoscience Letters, 2023. https://doi.org/10.1186/s40562-023-00287-6
83. Zhao-Liang, L. et al. Satellite-derived land surface temperature: Current status and perspectives. Remote Sensing of Environment 2013, 131. https://doi.org/10.1016/j.rse.2012.12.008
84. Zhang, Y. and Sun, L. Spatial-temporal impacts of urban land use land cover on land surface temperature: Case studies of two Canadian urban areas. International Journal of Applied Earth Observation and Geoinformation 2019, 75. https://doi.org/10.1016/j.jag.2018.10.005
85. Haynes, M. W. et al. Australian mean land-surface temperature. Geothermics 2018, 72. https://doi.org/10.1016/j.geothermics.2017.10.008
86. Pal, S. and Ziaul, S. Detection of land use and land cover change and land surface temperature in English Bazar urban centre. The Egyptian Journal of Remote Sensing and Space Sciences 2017, 20. https://doi.org/10.1016/j.ejrs.2016.11.003
87. Rawat, V. et al. Anomalous land surface temperature and outgoing long-wave radiation observations prior to earthquakes in India and Romania. Nat Hazards 2011, 59. https://doi.org/10.1007/s11069-011-9736-5
88. Li, Z. L. et al. Satellite remote sensing of global land surface temperature: Definition, methods, products, and applications. Reviews of Geophysics 2023, 61. https://doi.org/10.1029/2022RG000777
89. Voogt, J.A. and Oke, T. R. Effects of urban surface geometry on remotely-sensed surface temperature. Int. J. Remote Sens. 1998, 19. https://doi.org/10.1080/014311698215784
90. Voogt, J.A. and Oke, T. R. Complete Urban Surface Temperatures. J. Appl. Meteorol. 1997, 36. https://doi.org/10.1175/1520-0450(1997)036<1117:CUST>2.0.CO;2
91. Marzban, F. et al. Estimation of the Near-Surface Air Temperature during the Day and Nighttime from MODIS in Berlin, Germany. Int. J. Adv. Remote Sens. GIS 2018, 7. https://doi.org/10.23953/cloud.ijarsg.337
92. Good, E. et al. A spatiotemporal analysis of the relationship between near-surface air temperature and satellite land surface temperatures using 17 years of data from the ATSR series. Journal of Geophysical Research: Atmospheres 2017, 122. https://doi.org/10.1002/2017jd026880
93. Bhandari, R. et al. A Deep Neural Network-Based Approach for Studying the Relationship Between Land Surface Temperature and Surface Air Temperature. Journal of the Indian Society of Remote Sensing 2022, 50. https://doi.org/10.1007/s12524-021-01483-7

94. Arnfield, A. J. Two decades of urban climate research: a review of turbulence, exchanges of energy and water, and the urban heat island. International Journal of Climatology: a Journal of the Royal Meteorological Society 2003, 23. https://doi.org/10.1002/joc.859
95. Kloog, I. et al. Predicting spatiotemporal mean air temperature using MODIS satellite surface temperature measurements across the Northeastern USA. Remote Sens. Environ. 2014, 150. https://doi.org/10.1016/j.rse.2014.04.024
96. Oyler, J. W. et al. Creating a topoclimatic daily air temperature dataset for the conterminous United States using homogenized station data and remotely sensed land skin temperature. Int. J. Climatol. 2015, 35. https://doi.org/10.1002/joc.4127
97. Mildrexler, D. J. et al. A global comparison between station air temperatures and MODIS land surface temperatures reveals the cooling role of forests. J. Geophys. Res. Biogeosci. 2011, 116. https://doi.org/10.1029/2010JG001486
98. Benali, A. et al. Estimating air surface temperature in Portugal using MODIS LST data. Remote Sensing of Environment 2012, 124. https://doi.org/10.1016/j.rse.2012.04.024
99. Noi, P. T. et al. Comparison of Multiple Linear Regression, Cubist Regression, and Random Forest Algorithms to Estimate Daily Air Surface Temperature from Dynamic Combinations of MODIS LST Data. Remote Sens. 2017, 9. https://doi.org/10.3390/rs9050398
100. Rosselló, C. et al. Modeling air temperature through a combination of remote sensing and GIS data. Journal of Geophysical Research 2008, 113. https://doi.org/10.1029/2007JD009318
101. Pichierri, M. et al. Satellite air temperature estimation for monitoring the canopy layer heat island of Milan. Remote Sens. Environ. 2012, 127. https://doi.org/10.1016/j.rse.2012.08.025
102. Ho, H. C. et al. Mapping maximum urban air temperature on hot summer days. Remote Sensing of Environment 2014, 154. https://doi.org/10.1016/j.rse.2014.08.012
103. Ding, X. et al. Machine learning-assisted mapping of city-scale air temperature: Using sparse meteorological data for urban climate modeling and adaptation. Building and Environment 2023, 234. https://doi.org/10.1016/j.buildenv.2023.110211
104. Venter, Z. et al. Hyperlocal mapping of urban air temperature using remote sensing and crowdsourced weather data. Remote Sensing of Environment 2020, 242. https://doi.org/10.1016/j.rse.2020.111791
105. Howard, H. H. Computational Fluid Dynamics; In book: Fluid Mechanics, 2012. https://doi.org/10.1016/B978-0-12-382100-3.10010-1
106. Toparlar, Y. et al. A review on the CFD analysis of urban microclimate. Renewable and Sustainable Energy Reviews 2017, 80. https://doi.org/10.1016/j.rser.2017.05.248
107. Liu, Z. et al. Heat mitigation benefits of urban green and blue infrastructures: A systematic review of modeling techniques, validation and scenario simulation in ENVI-met V4. Building and Environment 2021, 200. https://doi.org/10.1016/j.buildenv.2021.107939
108. Yang, Y. et al. The "plant evaluation model" for the assessment of the impact of vegetation on outdoor microclimate in the urban environment. Building and Environment 2019, 159. https://doi.org/10.1016/j.buildenv.2019.05.029
109. Kumar, P. et al. Nature-based solutions efficiency evaluation against natural hazards: Modelling methods, advantages and limitations. Science of The Total Environment 2021, 784. https://doi.org/10.1016/j.scitotenv.2021.147058
110. Azmeer, A. et al. Progress on green infrastructure for urban cooling: Evaluating techniques, design strategies, and benefits. Urban Climate 2024, 56. https://doi.org/10.1016/j.uclim.2024.102077
111. Skamarock, W.C. and Klemp, J. B. A time-split nonhydrostatic atmospheric model for weather research and forecasting applications. Journal of Computational Physics 2008, 227. https://doi.org/10.1016/j.jcp.2007.01.037
112. Taha, H. Urban Climates and Heat Islands; Albedo, Evapotranspiration, and Anthropogenic Heat. Energy and Buildings 1997, 25.
113. Taha, H. et al. Residential cooling loads and the urban heat island—the effects of albedo. Building and Environment 1988, 23. https://doi.org/10.1016/0360-1323(88)90033-9
114. Shashua-Bar, L. et al. The cooling efficiency of urban landscape strategies in a hot dry climate. Landscape and Urban Planning 2009, 92. https://doi.org/10.1016/j.landurbplan.2009.04.005
115. Mariani, L. et al. Climatological analysis of the mitigating effect of vegetation on the urban heat island of Milan, Italy. Science of The Total Environment 2016, 569-570. https://doi.org/10.1016/j.scitotenv.2016.06.111
116. Oke, T. R. The micrometeorology of the urban forest. Philos. Trans. R. Soc. Lond. Ser. B Biol. Sci. 1989, 324. https://doi.org/10.1098/rstb.1989.0051
117. Armson, D. et al. The effect of tree shade and grass on surface and globe temperatures in an urban area. Urban For. Urban Green. 2012, 11. https://doi.org/10.1016/j.ufug.2012.05.002
118. Shashua-Bar, L. and Hoffman, M. E. The Green CTTC model for predicting the air temperature in small urban wooded sites. Building and Environment 2002, 37. https://doi.org/10.1016/S0360-1323(01)00120-2

119. Monteith, J. and Unsworth, M. Principles of Environmental Physics; Academic Press, an imprint of Elsevier, Oxford, 2013.
120. Gill, S. E. et al. Modelling water stress to urban amenity grass in Manchester UK under climate change and its potential impacts in reducing urban cooling. Urban For. Urban Green. 2013, 12. https://doi.org/10.1016/j.ufug.2013.03.005
121. Lloyd, M. K. et al. Isotopic clumping in wood as a proxy for photorespiration in trees. Proceedings of the National Academy of Sciences 2023, 120. https://doi.org/10.1073/pnas.2306736120
122. Santamouris, M. Cooling the cities - a review of reflective and green roof mitigation technologies to fight heat island and improve comfort in urban environments. Solar Energy 2014, 103. https://doi.org/10.1016/j.solener.2012.07.003
123. Bowler, D. E. et al. Urban greening to cool towns and cities: A systematic review of the empirical evidence. Landscape and urban planning 2010, 97. https://doi.org/10.1016/j.landurbplan.2010.05.006
124. Zhang, L. et al. Effects of the tree distribution and species on outdoor environment conditions in a hot summer and cold winter zone: A case study in Wuhan residential quarters. Building and Environment 2018, 130. https://doi.org/10.1016/j.buildenv.2017.12.014
125. Zhao, Q. et al. Impact of tree locations and arrangements on outdoor microclimates and human thermal comfort in an urban residential environment. Urban Forestry and Urban Greening 2018, 32. https://doi.org/10.1016/j.ufug.2018.03.022
126. McPherson, E. G. et al. Chicago's Urban Forest Ecosystem: Results of the Chicago Urban Forest Climate Project; Gen. Tech. Rep. NE-186. Radnor, PA: U.S. Department of Agriculture, Forest Service, Northernestern Forest Experiment Station, 1994.
127. Sun, R. and Chen, L. How can urban water bodies be designed for climate adaptation? Landscape and Urban Planning 2012, 105. https://doi.org/10.1016/j.landurbplan.2011.11.018
128. Adams, L.W. and Dove, L. E. Wildlife Reserves and Corridors in the Urban Environment: A Guide to Ecological Landscape Planning and Resource Conservation; National Institute for Urban Wildlife, 1989.
129. Webb, B.W. and Zhang, Y. Spatial and seasonal variability in the components of the river heat budget. Hydrol Process 1997, 11.
130. Hathway, E.A. and Sharples, S. The interaction of rivers and urban form in mitigating the urban heat island effect: a UK case study. Building and Environment 2012, 58. https://doi.org/10.1016/j.buildenv.2012.06.013
131. Theeuwes, N. E. et al. Modeling the influence of open water surfaces on the summertime temperature and thermal comfort in the city. J. Geophys. Res.: Atmos. 2013, 118. https://doi.org/10.1002/jgrd.50704
132. Hathway, E.A. and Sharples, S. The interaction of rivers and urban form in mitigating the urban heat island effect: a UK case study. Build. Environ. 2012, 58. https://doi.org/10.1016/j.buildenv.2012.06.013
133. Dong, J. et al. Modelling air temperature gradients across managed small streams in western Washington. Journal of Environmental Management 1998, 53. https://doi.org/10.1006/jema.1998.0217
134. Hipsey, M.R. and Sivapalan, M. Parameterizing the effect of a wind shelter on evaporation from small water bodies. Water Resources Research 2003, 39. https://doi.org/10.1029/2002WR001784
135. Jauregui, E. Influence of a large urban park on temperature and convective precipitation in a tropical city. Energy and Buildings 1990, 15. https://doi.org/10.1016/0378-7788(90)90021-A
136. Upmanis, H. et al. The influence of green areas on nocturnal temperatures in a high latitude city (Göteborg, Sweden). International Journal of Climatology 1998, 18. https://doi.org/10.1002/(SICI)1097-0088(199805)18:6<681::AID-JOC289>3.0.CO;2-L
137. Jusuf, S. et al. The influence of land use on the urban heat island in Singapore. Habitat International - HABITAT INT 2007, 31. https://doi.org/10.1016/j.habitatint.2007.02.006
138. Lin, W. et al. Calculating cooling extents of green parks using remote sensing: Method and test. Landscape and Urban Planning 2015, 134. https://doi.org/10.1016/j.landurbplan.2014.10.012
139. Eyster, H.N. and Beckage, B. Arboreal Urban Cooling Is Driven by Leaf Area Index, Leaf Boundary Layer Resistance, and Dry Leaf Mass per Leaf Area: Evidence from a System Dynamics Model. Atmosphere 2023, 14. https://doi.org/10.3390/atmos14030552
140. Li, H. et al. Harnessing cooling from urban trees: Interconnecting background climates, urban morphology, and tree traits. EGUsphere 2024 [preprint]. https://doi.org/10.5194/egusphere-2024-234
141. Trzeciak, M. and Sikorska, D. Application of UAV and ground measurements for urban vegetation cooling benefits assessment, Wilanów Palace case study. Scientific Review Engineering and Environmental Sciences 2024, 33. https://doi.org/10.22630/srees.5619
142. Su, Y. et al. Estimating the cooling effect magnitude of urban vegetation in different climate zones using multi-source remote sensing. Urban Climate 2022, 43. https://doi.org/10.1016/j.uclim.2022.101155
143. Yu, Z. et al. Strong contributions of local background climate to the cooling effect of urban green vegetation. Sci Rep 2018, 8. https://doi.org/10.1038/s41598-018-25296-w
144. Saaroni, H. and Ziv, B. The impact of a small lake on heat stress in a Mediterranean urban park: The case of Tel Aviv, Israel. International journal of biometeorology 2003, 47. https://doi.org/10.1007/s00484-003-0161-7

145. Pang, B. et al. How to plan urban green space in cold regions of China to achieve the best cooling efficiency. Urban Ecosystems 2022, 25. https://doi.org/10.1007/s11252-022-01202-1
146. Huang, R. et al. Cooling Effect of Green Space and Water on Urban Heat Island and the Perception of Residents: A Case Study of Xi'an City. International Journal of Environmental Research and Public Health (IJERPH) 2022, 19. https://doi.org/10.3390/ijerph192214880
147. Hirai, H. and Kitaya, Y. Effects of Gravity on Transpiration of Plant Leaves. Annals of the New York Academy of Sciences 2009, 1161. https://doi.org/10.1111/j.1749-6632.2009.04093.x
148. Zhaowu, Y. et al. Enhanced observations from an optimized soil-canopy-photosynthesis and energy flux model revealed evapotranspiration-shading cooling dynamics of urban vegetation during extreme heat. Remote Sensing of Environment 2024. https://doi.org/10.1016/j.rse.2024.114098
149. Jaganmohan, M. et al. The bigger, the better? The influence of urban green space design on cooling effects for residential areas. J. Environ. Qual. 2016, 45. https://doi.org/10.2134/jeq2015.01.0062
150. Keramitsoglou, I. et al. An online system for nowcasting satellite derived temperatures for urban areas. Remote Sens. 2016, 8. https://doi.org/10.3390/rs8040306
151. Cai, Y.-B. et al. Investigate the Difference of Cooling Effect between Water Bodies and Green Spaces: The Study of Fuzhou, China. Water 2022, 14. https://doi.org/10.3390/w14091471
152. Cao, B. et al. Simulation Analysis of the Cooling Effect of Urban Water Bodies on the Local Thermal Environment. Water 2022, 14. https://doi.org/10.3390/w14193091
153. Murakawa, S. et al. Study of the effects of a river on the thermal environment in an urban area. Energy Build. 1991, 16. https://doi.org/10.1016/0378-7788(91)90094-j
154. Hathway, E. and Sharples, S. The interaction of rivers and urban form in mitigating the Urban Heat Island effect: a UK case study. Build. Environ. 2012, 58. https://doi.org/10.1016/j.buildenv.2012.06.013
155. Ellison, D. et al. Trees, forests and water: cool insights for a hot world. Glob. Environ. Change. 2017, 43. https://doi.org/10.1016/j.gloenvcha.2017.01.002
156. Du, H. et al. A cold island connectivity and network perspective to mitigate the urban heat island effect. Sustainable Cities and Society 2023, 94. https://doi.org/10.1016/j.scs.2023.104525
157. Maimaitiyiming, M. et al. Effects of green space spatial pattern on land surface temperature: Implications for sustainable urban planning and climate change adaptation. ISPRS Journal of Photogrammetry and Remote Sensing 2014, 89. https://doi.org/10.1016/j.isprsjprs.2013.12.010
158. Bao, T. et al. Assessing the Distribution of Urban Green Spaces and its Anisotropic Cooling Distance on Urban Heat Island Pattern in Baotou, China. ISPRS Int. J. Geo-Inf. 2016, 5. https://doi.org/10.3390/ijgi5020012
159. Li, X. et al. Spatial pattern of greenspace affects land surface temperature: evidence from the heavily urbanized Beijing metropolitan area, China. Landscape Ecol 2012, 27. https://doi.org/10.1007/s10980-012-9731-6
160. Nasar-u-Minallah, M. et al. Evaluating the impact of landscape configuration, patterns and composition on land surface temperature: an urban heat island study in the Megacity Lahore, Pakistan. Environ Monit Assess 2024, 196. https://doi.org/10.1007/s10661-024-12758-0
161. Theeuwes, N. et al. Modeling the influence of open water surfaces on the summertime temperature and thermal comfort in the city. J. Geophys. Res. Atmos. 2013, 118. https://doi.org/10.1002/jgrd.50704
162. Liu, L. et al. Cooling effects of wetland parks in hot and humid areas based on remote sensing images and local climate zone scheme. Building and Environment 2023, 243. https://doi.org/10.1016/j.buildenv.2023.110660
163. Stewart, I.D. and Oke, T. Local Climate Zones for Urban Temperature Studies. Bulletin of the American Meteorological Society 2012, 93. https://doi.org/10.1175/BAMS-D-11-00019.1
164. Rogers, R. et al. Urban Task Force, Towards an Urban Renaissance: Final Report of the Urban Task Force Chaired by Lord Rogers of Riverside; Department of the Environment, Transport and the Regions, London, 1999.
165. Wong, N. H. et al. Investigation of Thermal Benefits of Rooftop Garden in the Tropical Environment. Building and Environment 2003, 38. https://doi.org/10.1016/S0360-1323(02)00066-5
166. Zhang, Y. et al. Analysis of cold island effect in city parks from the perspectives of maximum and cumulative values – a case study of Xi'an City. Archives of Environmental Protection 2024, 50. https://doi.org/10.24425/aep.2024.149436
167. Feyisa, G. L. et al. Efficiency of parks in mitigating urban heat island effect: An example from Addis Ababa. Landscape and Urban Planning 2014, 123. https://doi.org/10.1016/j.landurbplan.2013.12.008
168. Burton, E. Measuring urban compactness in UK towns and cities. Environment and Planning B: Planning and Design 2002, 29. https://doi.org/10.1068/b2713
169. McPherson, E. G. et al. Energy-efficient landscapes. In: Bradley, G. ed., Urban Forest Landscapes - Integrating Multidisciplinary Perspectives; University of Washington Press, Seattle, London, 1994.
170. Yang, X. et al. Air humidity characteristics of local climate zones: A three-year observational study in Nanjing. Building and Environment 2020, 175. https://doi.org/10.1016/j.buildenv.2020.106661

171. Zhao, Z. et al. Local Climate Zone Classification Scheme Can Also Indicate Local-Scale Urban Ventilation Performance: An Evidence-Based Study. Atmosphere 2020, 11. https://doi.org/10.3390/atmos11080776
172. Alexander, P.J. and Mills, G. Local Climate Classification and Dublin's Urban Heat Island. Atmosphere 2014, 5. https://doi.org/10.3390/atmos5040755
173. Ching, J. et al. World Urban Database and Access Portal Tools (WUDAPT), an urban weather, climate and environmental modeling infrastructure for the Anthropocene. Bulletin of the American Meteorological Society 2018, 99. https://doi.org/10.1175/BAMS-D-16-0236.1
174. Skarbit, N. et al. Airborne surface temperature differences of the different Local Climate Zones in the urban area of a medium sized city; Joint Urban Remote Sensing Event (JURSE), 2015. https://doi.org/10.1109/JURSE.2015.7120497
175. Geletič, J. et al. Land Surface Temperature Differences within Local Climate Zones, Based on Two Central European Cities. Remote sensing 2016, 8. https://doi.org/10.3390/rs8100788
176. Stewart, I. D. et al. Evaluation of the 'local climate zone' scheme using temperature observations and model simulations. International Journal of Climatology 2014, 34. https://doi.org/10.1002/joc.3746
177. Li, X. et al. The role of blue green infrastructure in the urban thermal environment across seasons and local climate zones in East Africa. Sustainable Cities and Society 2022, 80. https://doi.org/10.1016/j.scs.2022.103798
178. Geletič, J. et al. Inter-/intra-zonal seasonal variability of the surface urban heat island based on local climate zones in three central European cities. Building and Environment 2019, 156. https://doi.org/10.1016/j.buildenv.2019.04.011
179. Wang, Y. et al. Impact of Urban Climate Landscape Patterns on Land Surface Temperature in Wuhan, China. Sustainability 2017, 9. https://doi.org/10.3390/su9101700
180. Mohamed, A. A. et al. Land surface temperature and emissivity estimation for Urban Heat Island assessment using medium-and low-resolution space-borne sensors: A review. Geocarto international 2017, 32. https://doi.org/10.1080/10106049.2016.1155657
181. Gorgani, S. A. et al. The Relationship between NDVI and LST in the urban area of Mashhad, Iran; Conference: International Conference on Civil Engineering Architecture and Urban Sustainable Development, 2012.
182. Skelhorn, C. et al. The impact of vegetation types on air and surface temperatures in a temperate city: A fine scale assessment in Manchester, UK. Landscape and Urban Planning 2014, 121. https://doi.org/10.1016/j.landurbplan.2013.09.012
183. Sun, M. et al. Factors Affecting the High-Intensity Cooling Distance of Urban Green Spaces: A Case Study of Xi'an, China. Sustainability 2023, 15. https://doi.org/10.3390/su15086735
184. Huang, M. et al. Study of the Cooling Effects of Urban Green Space in Harbin in Terms of Reducing the Heat Island Effect. Sustainability 2018, 10. https://doi.org/10.3390/su10041101
185. Oliver, M.A. and Webster, R. Kriging: a method of interpolation for geographical information systems. International Journal of Geographical Information Systems 1990, 4. https://doi.org/10.1080/02693799008941549
186. NASA. Thematic Mapper (TM). Available on-line: https://landsat.gsfc.nasa.gov/thematic-mapper/ (accessed on 5.06.2024).
187. U.S. Geological Survey. Landsat-A Global Land-Imaging Mission: U.S. Geological Survey Fact Sheet 2012–3072: https://pubs.usgs.gov/fs/2012/3072/ (accessed on 5.06.2024).
188. Wolf, T. et al. Performance assessment of a heat wave vulnerability index for greater London, United Kingdom. Weather, climate, and society 2013. https://doi.org/10.1175/WCAS-D-13-00014.1
189. Tomlinson, C. J. et al. Including the urban heat island in spatial heat health risk assessment strategies: a case study for Birmingham, UK. International Journal of Health Geographics 2011, 10.
190. Morabito, M. et al. Urban-Hazard Risk Analysis: Mapping of Heat-Related Risks in the Elderly in Major Italian Cities. Plos one 2014. https://doi.org/10.1371/journal.pone.0127277
191. Imhoff, M. L. et al. Remote sensing of the urban heat island effect across biomes in the continental USA. Remote sensing of environment 2010, 114. https://doi.org/10.1016/j.rse.2009.10.008
192. Peng, S. et al. Surface Urban Heat Island Across 419 Global Big Cities. Environmental Science and Technology 2012, 46. https://doi.org/10.1021/es2030438
193. Wan, Z. et al. Early Land-Surface Temperature Product Retrieved from MODIS Data. IGARSS 2001. Available online: https://bit.ly/2V3SllY (accessed on 10.07.2024).
194. Wan, Z. and Dozier, J. A generalized split-window algorithm for retrieving land-surface temperature from space. IEEE Transactions on Geoscience and Remote Sensing 1996, 34. https://doi.org/10.1109/36.508406
195. Yamaguchi, Y. et al. Overview of Advanced Spaceborne Thermal Emission and Reflection Radiometer (ASTER). Transactions on Geoscience and Remote Sensing 1998, 36. https://doi.org/10.1109/36.700991
196. Abrams, M. The Advanced Spaceborne Thermal Emission and Reflection Radiometer (ASTER): Data products for the high spatial resolution imager on NASA's Terra platform. International Journal of Remote Sensing 2000, 21. https://doi.org/10.1080/014311600210326

197. Zheng, B. et al. Spatial configuration of anthropogenic land cover impacts on urban warming. Landscape and Urban Planning 2014, 130. https://doi.org/10.1016/j.landurbplan.2014.07.001
198. Wei, L. and Sobrino, J. A. Surface urban heat island analysis based on local climate zones using ECOSTRESS and Landsat data: A case study of Valencia city (Spain). International Journal of Applied Earth Observation and Geoinformation 2024, 130. https://doi.org/10.1016/j.jag.2024.103875
199. Chang, Y. et al. Exploring diurnal thermal variations in urban local climate zones with ECOSTRESS land surface temperature data. Remote Sensing of Environment 2021, 263. https://doi.org/10.1016/j.rse.2021.112544
200. Hulley, G. and Freepartner, R. ECOsystem Spaceborne Thermal Radiometer Experiment on Space Station (ECOSTRESS) Mission. Level 2 Product User Guide. Available on-line: https://lpdaac.usgs.gov/documents/423/ECO2_User_Guide_V1.pdf (accessed on 19.06.2024)
201. Oltra-Carrió, R. et al. Land surface emissivity retrieval from airborne sensor over urban areas. Remote Sensing of Environment 2012, 123. https://doi.org/10.1016/j.rse.2012.03.007
202. Shah, A. et al. Quantifying the local cooling effects of urban green spaces: Evidence from Bengaluru, India. Landscape and Urban Planning 2021, 209. https://doi.org/10.1016/j.landurbplan.2021.104043
203. Garcia-Haro, A. et al. Quantifying the influence of design and location on the cool island effect of the urban parks of Barcelona. Journal of Applied Remote Sensing 2023. https://doi.org/10.1117/1.JRS.17.034512
204. Xue, Z. et al. Quantifying the cooling-effects of urban and peri-urban wetlands using remote sensing data: Case study of cities of Northeast China. Landscape and Urban Planning 2019, 182. https://doi.org/10.1016/j.landurbplan.2018.10.015
205. Cao, X. et al. Quantifying the cool island intensity of urban parks using ASTER and IKONOS data. Landscape and Urban Planning 2010, 96. https://doi.org/10.1016/j.landurbplan.2010.03.008
206. Zhao, W. et al. An improved method for assessing vegetation cooling service in regulating thermal environment: A case study in Xiamen, China. Ecological Indicators 2019, 98. https://doi.org/10.1016/j.ecolind.2018.11.033
207. Mirzaei, P.A. Recent challenges in modeling of urban heat island. Sustainable Cities and Society 2015, 19. https://doi.org/10.1016/j.scs.2015.04.001
208. Bruse, M. and Fleer, H. Simulating surface–plant–air interactions inside urban environments with a three dimensional numerical model. Environmental Modelling and Software 1998, 13. https://doi.org/10.1016/S1364-8152(98)00042-5
209. Tsoka, S. et al. Analyzing the ENVI-met microclimate model's performance and assessing cool materials and urban vegetation applications–A review. Sustainable Cities and Society 2018, 43. https://doi.org/10.1016/j.scs.2018.08.009
210. Lee, H. et al. Contribution of trees and grasslands to the mitigation of human heat stress in a residential district of Freiburg, Southwest Germany. Landscape and Urban Planning 2016, 148. https://doi.org/10.1016/j.landurbplan.2015.12.004
211. Kleerekoper, L. et al. Urban measures for hot weather conditions in a temperate climate condition: A review study. Renewable and Sustainable Energy Reviews 2017, 75. https://doi.org/10.1016/j.rser.2016.11.019
212. Acero, J.A. and Herranz-Pascual, K. A comparison of thermal comfort conditions in four urban spaces by means of measurements and modelling techniques. Building and Environment 2015, 93. https://doi.org/10.1016/j.buildenv.2015.06.028
213. Acero, J.A. and Arrizabalaga, J. Evaluating the performance of ENVI-met model in diurnal cycles for different meteorological conditions. Theor Appl Climatol 2018, 131. https://doi.org/10.1007/s00704-016-1971-y
214. Morakinyo, T. E. et al. A study on the impact of shadow-cast and tree species on in-canyon and neighborhood's thermal comfort. Building and Environment 2017, 115. https://doi.org/10.1016/j.buildenv.2017.01.005
215. Ladybug Tools. Available on-line: https://www.ladybug.tools/ (accessed on 15.08.2024)
216. Roudsari, M.S. and Pak, M. Ladybug: A parametric environmental plugin for grasshopper to help designers create an environmentally-conscious design; 13th Conference of International Building Performance Simulation Association, Chambéry, France, 2012.
217. Simon, H. Modeling urban microclimate : development, implementation and evaluation of new and improved calculation methods for the urban microclimate model ENVI-met. Environmental Science, Engineering 2016.
218. Jacobs, C. et al. Are urban water bodies really cooling? Urban Climate 2020, 32. https://doi.org/10.1016/j.uclim.2020.100607
219. Jamei, E. Review on the impact of urban geometry and pedestrian level greening on outdoor thermal comfort. Renewable and Sustainable Energy Reviews 2015, 54. https://doi.org/10.1016/j.rser.2015.10.104
220. Ng, E. et al. A study on the cooling effects of greening in a high-density city: an experience from Hong Kong. Building and Environment 2012, 47. https://doi.org/10.1016/j.buildenv.2011.07.014

221. Middel, A. et al. Urban forestry and cool roofs: Assessment of heat mitigation strategies in Phoenix residential neighborhoods. Urban Forestry and Urban Greening 2015, 14. https://doi.org/10.1016/j.ufug.2014.09.010
222. Wang, Y. et al. Comparing the effects of urban heat island mitigation strategies for Toronto, Canada. Energy and Buildings 2016, 114. https://doi.org/10.1016/j.enbuild.2015.06.046
223. Berardi, U. et al. Effects of greenery enhancements for the resilience to heat waves: a comparison of analysis performed through mesoscale (WRF) and microscale (Envi-met) modeling. Sci. Total Environ. 2020, 747. https://doi.org/10.1016/j.scitotenv.2020.141300
224. Herath, H. M. P. I. K. et al. Evaluation of green infrastructure effects on tropical Sri Lankan urban context as an urban heat island adaptation strategy. Urban For. Urban Green. 2018, 29. https://doi.org/10.1016/j.ufug.2017.11.013
225. Morakinyo, T. E. et al. Temperature and cooling demand reduction by green-roof types in different climates and urban densities: a co-simulation parametric study. Energy Build. 2017, 145. https://doi.org/10.1016/j.enbuild.2017.03.066
226. Taleghani, M. et al. Micrometeorological simulations to predict the impacts of heat mitigation strategies on pedestrian thermal comfort in a Los Angeles neighborhood. Environ. Res. Lett. 2016, 11. https://doi.org/10.1088/1748-9326/11/2/024003
227. Declet-Barreto, J. et al. Creating the park cool island in an inner-city neighborhood: heat mitigation strategy for Phoenix, AZ. Urban Ecosyst. 2013, 16. https://doi.org/10.1007/s11252-012-0278-8
228. Ziaul, S. and Pal, S. Modeling the effects of green alternative on heat island mitigation of a Meso level town, West Bengal, India. Adv. Space Res. 2020, 65. https://doi.org/10.1016/j.asr.2019.12.031
229. Błażejczyk, K. et al. An introduction to the Universal Thermal Climate Index (UTCI). Geographia Polonica 2012, 86. https://doi.org/10.7163/GPol.2013.1.
230. Declet-Barreto, J. et al. Creating the park cool island in an inner-city neighborhood: heat mitigation strategy for Phoenix, AZ. Urban Ecosystems 2013, 16. https://doi.org/10.1007/s11252-012-0278-8
231. Heldens, W. et al. Potential of hyperspectral data for urban micro climate analysis; Hyperspectral Workshop 2010.
232. Vidrih, B. and Medved, S. Multiparametric model of urban park cooling island. Urban Forestry and Urban Greening 2013, 12. https://doi.org/10.1016/j.ufug.2013.01.002
233. Ghaffarianhoseini, A. et al. Thermal performance characteristics of unshaded courtyards in hot and humid climates. Build. Environ. 2015, 87. https://doi.org/10.1016/j.buildenv.2015.02.001
234. Lin, B-S. and Lin, C-T. Preliminary study of the influence of the spatial arrangement of urban parks on local temperature reduction. Urban Forestry and Urban Greening 2016, 20. https://doi.org/10.1016/j.ufug.2016.10.003
235. Santamouris, M. et al. On the energy impact of urban heat island in Sydney: climate and energy potential of mitigation technologies. Energy Build. 2018, 166. https://doi.org/10.1016/j.enbuild.2018.02.007
236. Salata, F. et al. Relating microclimate, human thermal comfort and health during heat waves: an analysis of heat island mitigation strategies through a case study in an urban outdoor environment. Sustain. Cities Soc. 2017, 30. https://doi.org/10.1016/j.scs.2017.01.006
237. Mohammed, A. et al. Numerical evaluation of enhanced green infrastructures for mitigating urban heat in a desert urban setting. Build. Simul. 2023, 16. https://doi.org/10.1007/s12273-022-0940-x
238. Sharma, A. et al. Green and cool roofs to mitigate urban heat island effects in the Chicago metropolitan area: evaluation with a regional climate model. Environ. Res. Lett. 2016, 11. https://doi.org/10.1088/1748-9326/11/6/064004
239. Khan, A. et al. Urban cooling potential and cost comparison of heat mitigation techniques for their impact on the lower atmosphere. Computational Urban Science 2023, 3. https://doi.org/10.1007/s43762-023-00101-1
240. Haddad, S. et al. Quantifying the energy impact of heat mitigation technologies at the urban scale. Nat Cities 2024, 1. https://doi.org/10.1038/s44284-023-00005-5
241. Khan, A. et al. On the mitigation potential and urban climate impact of increased green infrastructures in a coastal mediterranean city. Building and Environment 2022, 221. https://doi.org/10.1016/j.buildenv.2022.109264
242. Fu, J. et al. Optimized greenery configuration to mitigate urban heat: a decade systematic review. Front. Archit. Res. 2022. https://doi.org/10.1016/j.foar.2021.12.005
243. Vaz Monteiro, M. et al. The impact of greenspace size on the extent of local nocturnal air temperature cooling in London. Urban Forestry and Urban Greening 2016, 16. https://doi.org/10.1016/j.ufug.2016.02.008
244. Qi, Q. et al. Applicability of mobile-measurement strategies to different periods: A field campaign in a precinct with a block park. Building and Environment 2022, 211. https://doi.org/10.1016/j.buildenv.2022.108762

245. Yan, C. et al. Quantifying the cooling effect of urban vegetation by mobile traverse method: A local-scale urban heat island study in a subtropical megacity. Building and Environment 2020, 169. https://doi.org/10.1016/j.buildenv.2019.106541
246. Hoelscher, M.-T. et al. Quantifying cooling effects of facade greening: Shading, transpiration and insulation. Energy and Buildings 2016, 114. https://doi.org/10.1016/j.enbuild.2015.06.047
247. Hamada, S. and Ohta, T. Seasonal variations in the cooling effect of urban green areas on surrounding urban areas. Urban Forestry and Urban Greening 2010, 9. https://doi.org/10.1016/j.ufug.2009.10.002
248. Mei, C. et al. Integrated assessments of green infrastructure for flood mitigation to support robust decision-making for sponge city construction in an urbanized watershed. Science of The Total Environment 2018, 639. https://doi.org/10.1016/j.scitotenv.2018.05.199
249. Wu, X. et al. Assessing the performance of blue-green solutions through a fine-scale water balance model for an urban area. Science of The Total Environment 2024, 948. https://doi.org/10.1016/j.scitotenv.2024.174750
250. Taha, H. Cool cities: counteracting potential climate change and its health impacts. Curr. Clim. Chang. Rep. 2015, 1. https://doi.org/10.1007/s40641-015-0019-1
251. Mata, L. et al. Large positive ecological changes of small urban greening actions. Ecological Solutions and Evidence 2023, 4. https://doi.org/10.1002/2688-8319.12259
252. Mohammed, A. et al. Numerical evaluation of enhanced green infrastructures for mitigating urban heat in a desert urban setting. Build. Simul. 2023, 16. https://doi.org/10.1007/s12273-022-0940-x
253. VanDerHorn, E. and Mahadevan, S. Digital Twin: Generalization, characterization and implementation. Decision Support Systems 2021, 145. https://doi.org/10.1016/j.dss.2021.113524
254. Weil, C. et al. Urban Digital Twin Challenges: A Systematic Review and Perspectives for Sustainable Smart Cities. Sustainable Cities and Society 2023, 99. https://doi.org/10.1016/j.scs.2023.104862
255. Ferré-Bigorra, J. et al. The adoption of urban digital twins. Cities 2022, 131.
256. Ruohomäki, T. et al. Smart City Platform Enabling Digital Twin; 2018 International Conference on Intelligent Systems (IS), 2018. https://doi.org/10.1109/IS.2018.8710517
257. Schrotter, G. and Hürzeler, C. The Digital Twin of the City of Zurich for Urban Planning. PFG 2020, 88. https://doi.org/10.1007/s41064-020-00092-2
258. Ketzler, B. et al. Digital Twins for Cities: A State of the Art Review. built environ 2020, 46. https://doi.org/10.2148/benv.46.4.547
259. Sahahat, E. et al. City Digital Twin Potentials: A Review and Research Agenda. Sustainability 2021, 13. https://doi.org/10.3390/su13063386
260. Tomin, N. et al. Development of Digital Twin for Load Center on the Example of Distribution Network of an Urban District. E3S Web Conf. 2020, 209. https://doi.org/10.1051/e3sconf/202020902029
261. Bibri, S. E. et al. Environmentally Sustainable Smart Cities and their Converging AI, IoT, and Big Data Technologies and Solutions: An Integrated Approach to an Extensive Literature Review. Energy Informatics 2023, 6. https://doi.org/10.1186/s42162-023-00259-2
262. Eicker, U. et al. On the design of an urban data and modeling platform and its application to urban district analyses. Energy and Buildings 2020, 217. https://doi.org/10.1016/j.enbuild.2020.109954
263. Nochta, T. et al. A Socio-Technical Perspective on Urban Analytics: The Case of City-Scale Digital Twins. J. Urban Technol. 2021, 28. https://doi.org/10.1080/10630732.2020.1798177
264. Boje, C. et al. Towards a semantic Construction Digital Twin: Directions for future research. Automation in Construction 2020, 114. https://doi.org/10.1016/j.autcon.2020.103179
265. Naserentin, V. et al. Combining Open Source and Commercial Tools in Digital Twin for Cities Generation. IFAC Workshop on Control for Smart Cities CSC 2022 2022, 55. https://doi.org/10.1016/j.ifacol.2022.08.070
266. Austin, M. et al. Architecting Smart City Digital Twins: Combined Semantic Model and Machine Learning Approach. Journal of Management in Engineering 2020, 36. https://doi.org/10.1061/(ASCE)ME.1943-5479.0000774
267. Saeed, Z. O. et al. Future City, Digital Twinning and the Urban Realm: A Systematic Literature Review. Buildings 2022, 12. https://doi.org/10.3390/buildings12050685
268. Gessa, A. and Sancha, P. Environmental Open Data in Urban Platforms: An Approach to the Big Data Life Cycle. Journal of Urban Technology 2020, 27. https://doi.org/10.1080/10630732.2019.1656934
269. Raes, L. et al. DUET: A Framework for Building Interoperable and Trusted Digital Twins of Smart Cities. IEEE Internet Computing 2022, 26. https://doi.org/10.1109/MIC.2021.3060962
270. Deng, T. et al. A systematic review of a digital twin city: A new pattern of urban governance toward smart cities. Journal of Management Science and Engineering 2021, 6. https://doi.org/10.1016/j.jmse.2021.03.003
271. Kikuchi, N. et al. Future landscape visualization using a city digital twin: integration of augmented reality and drones with implementation of 3D model-based occlusion handling. Journal of Computational Design and Engineering 2022, 9. https://doi.org/10.1093/jcde/qwac032
272. White, G. et al. A digital twin smart city for citizen feedback. Cities 2021, 110. https://doi.org/10.1016/j.cities.2020.103064

273. Wu, Y. et al. Digital Twin Networks: A Survey. IEEE Internet of Things Journal 2021, 8. https://doi.org/10.1109/JIOT.2021.3079510
274. Batty, M. Digital Twins. Environment and Planning B: Urban Analytics and City Science 2018, 45. https://doi.org/10.1177/2399808318796416
275. Brasil, J. A. T. et al. Can we scale Digital Twins of Nature-based Solutions for stormwater and transboundary water security projects? Journal of Hydroinformatics 2022, 24. https://doi.org/10.2166/hydro.2022.142
276. Dembski, F. et al. Urban Digital Twins for Smart Cities and Citizens: The Case Study of Herrenberg. Sustainability 2020, 12. https://doi.org/10.3390/su12062307
277. Marcucci, E. et al. Digital Twins: A Critical Discussion on Their Potential for Supporting Policy-Making and Planning in Urban Logistics. Sustainability 2020, 12. https://doi.org/10.3390/su122410623
278. Leal Filho, W. et al. Deploying artificial intelligence for climate change adaptation. Technological Forecasting and Social Change 2022, 180. https://doi.org/10.1016/j.techfore.2022.121662
279. Pan, H. et al. Contribution of prioritized urban nature-based solutions allocation to carbon neutrality. Nat. Clim. Chang. 2023, 13. https://doi.org/10.1038/s41558-023-01737-x
280. Saaroni, H. et al. Urban Green Infrastructure as a tool for urban heat mitigation: Survey of research methodologies and findings across different climatic regions. Urban Climate 2018, 24. https://doi.org/10.1016/j.uclim.2018.02.001
281. Colunga, M. L. et al. The role of urban vegetation in temperature and heat island effects in Querétaro city, Mexico. Atmósfera 2015, 28. https://doi.org/10.20937/ATM.2015.28.03.05
282. Demuzere, M. et al. LCZ Generator: a web application to create Local Climate Zone maps. Frontiers in Environmental Science 2021, 9. https://doi.org/10.3389/fenvs.2021.637455
283. Blaschke, T. et al. Geographic Object-Based Image Analysis – Towards a new paradigm. ISPRS Journal of Photogrammetry and Remote Sensing 2014, 87. https://doi.org/10.1016/j.isprsjprs.2013.09.014
284. Hay, G.J. and Castilla, G. Geographic Object-Based Image Analysis (GEOBIA): A new name for a new discipline; Springer, Berlin, 2008. https://doi.org/10.1007/978-3-540-77058-9_4
285. Smith, P. et al. Study of the urban microclimate using thermal UAV. The case of the mid-sized cities of Arica (arid) and Curicó (Mediterranean), Chile. Building and Environment 2021, 206. https://doi.org/10.1016/j.buildenv.2021.108372
286. Budzik, G. et al. Factors influencing spatiotemporal cooling potential of blue–green infrastructure across diverse local climate zones—Case study of Wroclaw, Poland. Building and Environment 2025, 267. https://doi.org/10.1016/j.buildenv.2024.112162
287. Liu, Z. et al. Accurate and efficient urban wind prediction at city-scale with memory-scalable graph neural network. Sustainable Cities and Society 2023, 99. https://doi.org/10.1016/j.scs.2023.104935